UVSOR

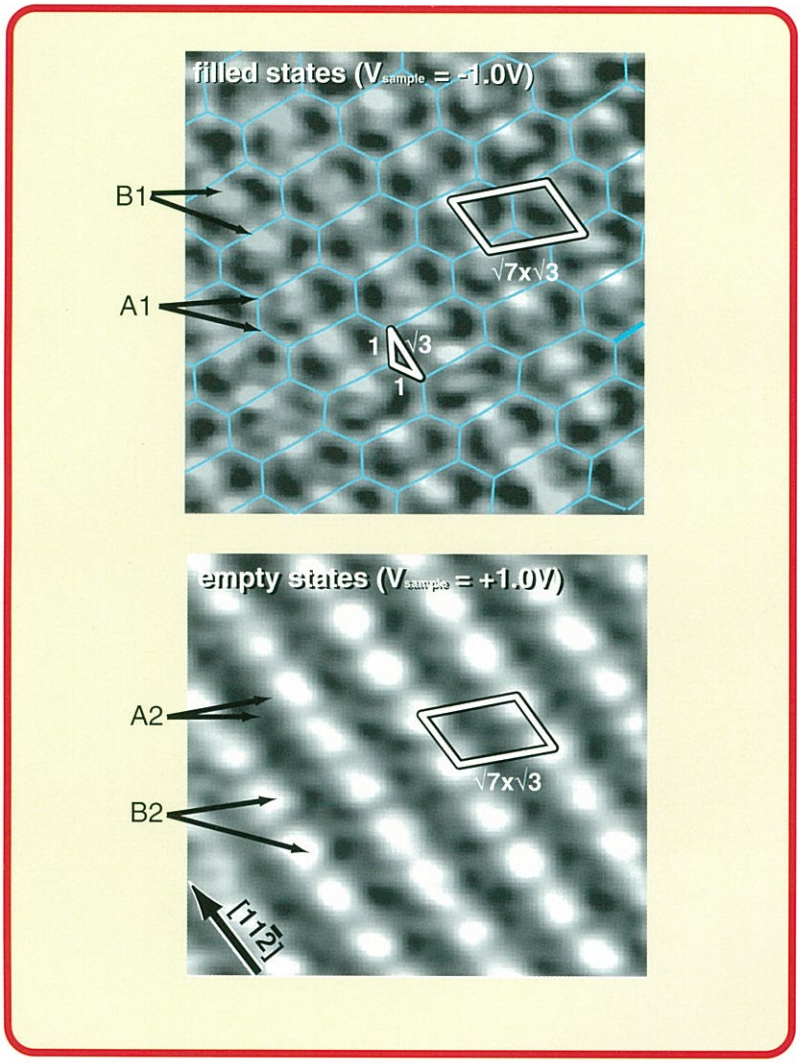

Solid State Spectroscopy II

(XAFS, PES)

BL1A, 5A, 5B, 6A2, 7A, 8B1, 8B2

(BL7A)

Oxidation State of Nickel Ion in Li_xNiO_2 from L-edge Spectroscopy

Takeshi YAO, Naoshi OZAWA, Hiroshi SAWADA and Yoshiharu UCHIMOTO

Department of Fundamental Energy Science
Graduate School of Energy Science
Kyoto University
Yoshida, Sakyo-ku, KYOTO 606-8501 Japan

Secondary lithium batteries using intercalation compounds as the cathode active material have been studied intensively. Among many intercalation compounds, $LiNiO_2$ with layer rock salt structure is one of the most promising cathode material used in lithium ion batteries. It is important to study valency change during charge and discharge process in order to understand their electrochemical properties. In this study, oxidation states of nickel ion in Li_xNiO_2 were determined by using a measurement of Ni L_{23}-edge X-ray absorption near edge structure.

A mixture of Li(OH) and $Ni(OH)_2$ in a mole ratio of 1:1 was heat-treated and $LiNiO_2$ was obtained. The crystal structure of the product was determined by XRD using MoKα radiation to confirm the formation of well characterized $LiNiO_2$. By electrochemical extraction of lithium ion, samples having various x values in Li_xNiO_2 were obtained.

Figure 1 shows the Ni L-edge X-ray absorption spectrum of Li_xNiO_2. The spectra were all attributed to the bivalent nickel ion in high spin state[1]. The change in the shapes of spectra was not so remarkable, it is considered that the valence state of the nickel ion was not changed with the change of the amount of lithium ion. In figure 2, the area ratio of the two sub-peaks in L3-edge (A and B in figure 1) is shown. It is shown that the ratio:B/A increase with the decrease of x, and this indicates that the nickel ion was oxidized with the extraction of lithium ion. It can be concluded that the valence state of the nickel ion was basically unchanged and was bivalent, but slightly oxidized with the extraction of lithium ion.

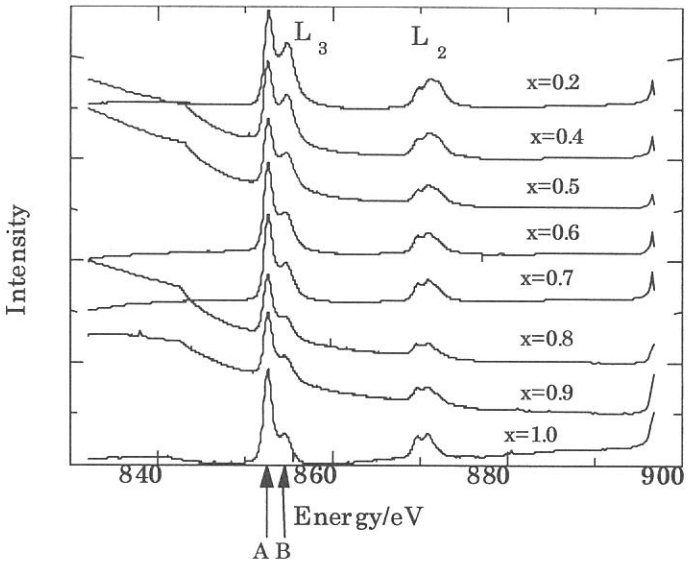

Figure 1 Ni L-edge XANES of Li_xNiO_2

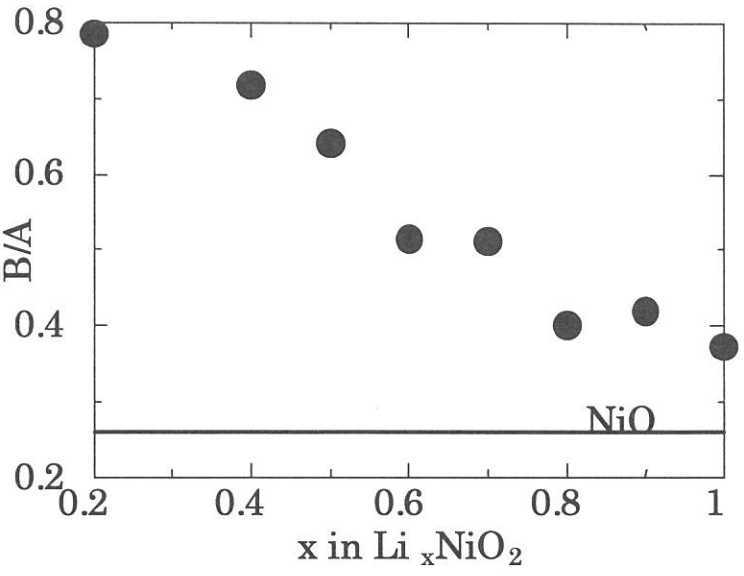

Figure 2 The area ratio of the two sub-peaks in L_3-edge (A and B in figure 1)

Reference
[1] L. A. Montoro, M. Abbate, J.M. Rosolen, J. Electrochem. Soc., **147**, 1651-1657 (2000)

(BL1A)

Ni 2p Photoabsorption and Resonant Photoelectron Spectroscopy of High-spin Ni complex, Ni(*N*,*N*'-dimethylethylenediamine)$_2$Cl$_2$

Hiroshi Oji, Yasutaka Takata, Takaki Hatsui, and Nobuhiro Kosugi

Institute for Molecular Science, Myodaiji, Okazaki 444-8585, JAPAN

In the previous study, we found that the planar Ni complexes with a $3d^8$ low-spin ground state show characteristic resonant behavior in the Ni 3p and 3s resonant photoelectron spectra, which is different from the resonant behaviors of Ni metal and Ni oxide.[1] The kinetic energy of Ni 3p satellite peaks decrease as the photon energy increases, indicating the one electron, or excitonic, feature of the excited states in these systems. In the present study, we measured soft X-ray Ni 2p absorption and resonant Ni 3s and 3p photoelectron spectra of a $3d^8$ high-spin Ni complex, Ni(*N*,*N*'-dimethylethylenediamine)$_2$Cl$_2$ (Ni(DED)$_2$Cl$_2$) to clarify the effect of the spin state on the core-excited states of the system.

For the measurement, the powder of Ni(DED)$_2$Cl$_2$ was compressed into the disk-form, which was fixed to the sample folder by conductive adhesion tape. Measurements of X-ray absorption and photoelectron spectra were performed at BL1A soft X-ray beamline of the UVSOR facility, equipped with the double crystal monochromator. A pair of beryl ($10\bar{1}0$) crystal was used for the monochromator crystal, where the bandpass of monochromatized light was 0.6 eV around the Ni 2p edge. The X-ray absorption spectra (XAS) were measured by the total electron yield mode. A SCIENTA SES-200 hemispherical electron energy analyzer was used for the measurement of photoelectron spectra. The energy resolution of the analyzer was ~0.4 eV and the total energy resolution for the measurements of the photoelectron spectra was ~0.7 eV. The photoelectron spectra of the Cl 2p region were measured to calibrate the electron energy and intensity of the spectra.

The Ni 2p X-ray absorption spectra of Ni(DED)$_2$Cl$_2$ is shown in Fig. 1. At the photon energy labeled as 0-8 in Fig. 1, the off- and on-resonant Ni 3p, 3s photoelectron spectra were measured, as shown in Fig.2. The normal Auger spectra measured at the photon energy of 899.8 eV and 1347.6 eV are also indicated in the upper part of the Fig. 2. Ni 3p and 3s primary ion states labeled with asterisk (*) are not enhanced through the resonant excitation. On the other hand, satellite peaks in the Ni 3p and 3s region (a-g) are enhanced through the resonant excitation. The trend of kinetic energy shift for these satellite peaks are similar to that of primary ion states, indicating their constant binding energy feature. To examine the trend of kinetic energy shift in detail, we have plotted the kinetic energy for the primary ion states and satellite peaks as a function of the photon energy in Fig. 3. This shows nearly linear relationship between the kinetic energy of these satellite peaks and the photon energy with the slope ($\Delta KE/\Delta h\nu$) of +1. This dependence of satellite bands on the photon energy is different from that of the low-spin complexes where the slope becomes negative (e.g. $\Delta KE/\Delta h\nu = -0.55\pm0.05$ for $K_2[Ni(CN)_4]$[1]), but is similar to that of NiO where the electron correlation and multiplet interaction are important. This indicates that the excited states in this high-spin Ni complex cannot be described by the one-electron picture. A series of our studies on the Ni complexes with various electronic states reveals that the resonant behavior of photoelectron spectra reflects the electron configuration of core-excited metal atom which depends on the chemical bonding

state between the metal and the ligand molecules.

Reference

1) Y. Takata, T. Hatsui, and N. Kosugi, *J. Electron Spectrosc. Relat. Phenom.* **88**, 235 (1998).

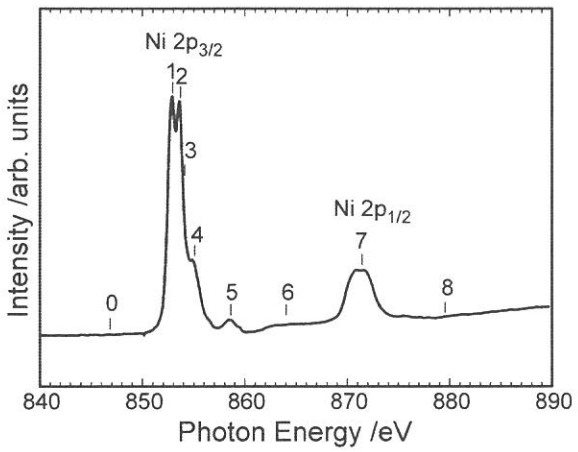

Fig. 1. Photoabsorption spectra at the Ni $2p_{3/2}$ and $2p_{1/2}$ edges for $Ni(DED)_2Cl_2$.

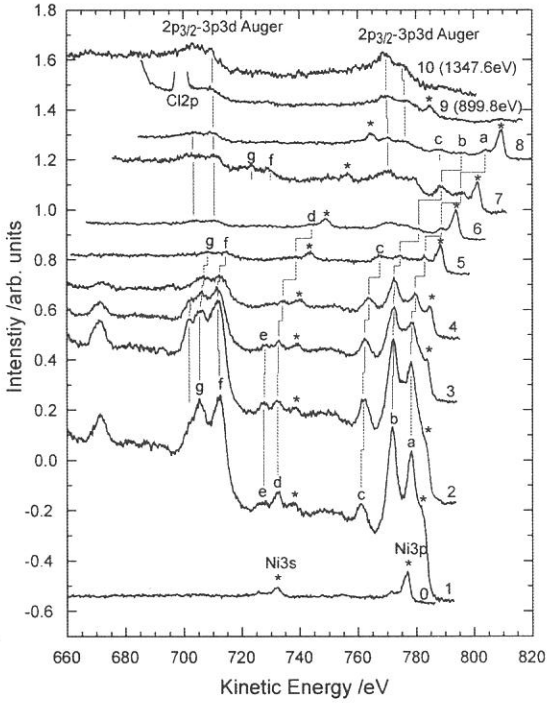

Fig. 2. Off- and on-resonant photoelectron spectra in the Ni 3p and 3s regions at the Ni $2p_{3/2}$ and $2p_{1/2}$ edges for $Ni(DED)_2Cl_2$.

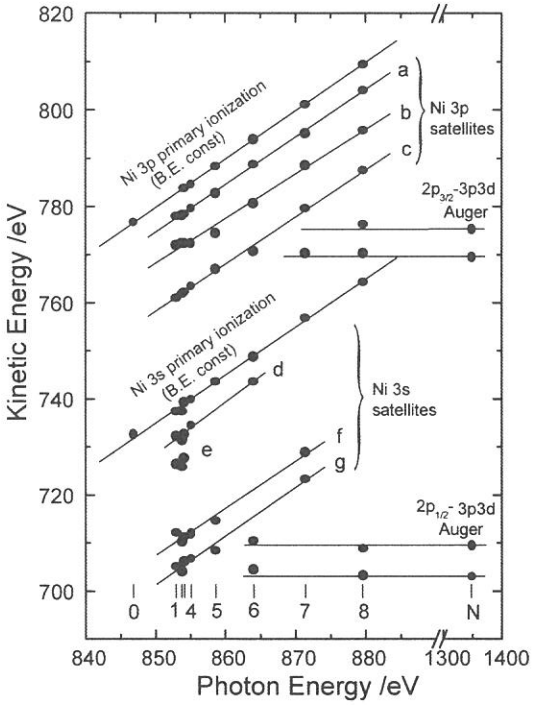

Fig. 3. Photon energy dependence of the kinetic energy for Ni 3p, 3s primary and satellite photoelectron peaks.

(BL5A)

Sn4*d* and Pb5*d* Core-level Photoelectron Spectra of Si(111) $\sqrt{7}\times\sqrt{3}$-(Pb, Sn) Surface

Kazuo SODA, Junji YUHARA, Takashi TAKADA, Osamu YOSHIMOTO, Masahiko KATO, Shinya YAGI, Kenji MORITA and *Masao KAMADA

Graduate School of Engineering, Nagoya University, Furo-cho, Chikusa-ku, Nagoya 464-8603

**UVSOR, Institute for Molecular Science, Myodaiji, Okazaki 444-8585*

Binary adsorbate system on a surface has a possibility of showing new atomic arrangement and properties such as thermal stability, electronic transport, film growth, preferential segregation and so on, which are different from those of single adsorbate system [1]. Recently we have found, by using combined techniques of scanning tunneling microscopy (STM), low energy electron diffraction (LEED), and Rutherford backscattering spectroscopy (RBS), that the coadsorption of Pb and Sn on the Si(111) surface forms a $\sqrt{7}\times\sqrt{3}$ superstructure at coverages of 0.4 ML Pb and 0.4 ML Sn and that Pb atoms on this surface become more stable against heating than those on single adsorbate system [2,3]. Here, 1 ML is defined as 7.8×10^{14} atoms/cm^2. As shown in Fig.1, the STM images of the surface consist of two kinds of bright spots: (A) those aligned zigzag on the T_1 site and (B) those on the T_1 and H_3 sites along the [112] direction. In this study, we have measured the Pb 5*d* and Sn 4*d* photoelectron spectra of the Si(111) $\sqrt{7}\times\sqrt{3}$-(Pb, Sn) surface in order to clarify their bonding properties and the atomic arrangement of the surface.

The Si(111) $\sqrt{7}\times\sqrt{3}$-(Pb, Sn) surface was prepared on a substrate of an n-type Si(111) wafer of 5 Ωcm in a size of $5\times20\times0.5$ mm^3 by annealing at 570 K after depositing about 1 ML Pb onto the Si(111) $\sqrt{3}\times\sqrt{3}$+faint $2\sqrt{3}\times2\sqrt{3}$-Sn surface with the Sn coverage of 0.4 ML, which was made by deposition of 1 ML Sn onto the clean Si(111) 7×7 surface and subsequent annealing at 970 K. Photoelectron measurement was performed at room temperature with the excitation photons of 52 eV and a hemi-spherical analyzer of the angle acceptance of $\pm1^\circ$ at the 45° emission angle. The origin of the binding energy was determined from the Fermi edge of a Ta plate which holds the Si wafer. Total energy resolution was also estimated to be about 0.1 eV from the Ta Fermi edge.

Typical spectra of the Pb 5*d* and Sn 4*d* levels of the Si(111) $\sqrt{7}\times\sqrt{3}$-(Pb, Sn) surface are shown in Figs. 2 and 3 in comparison with those for the single

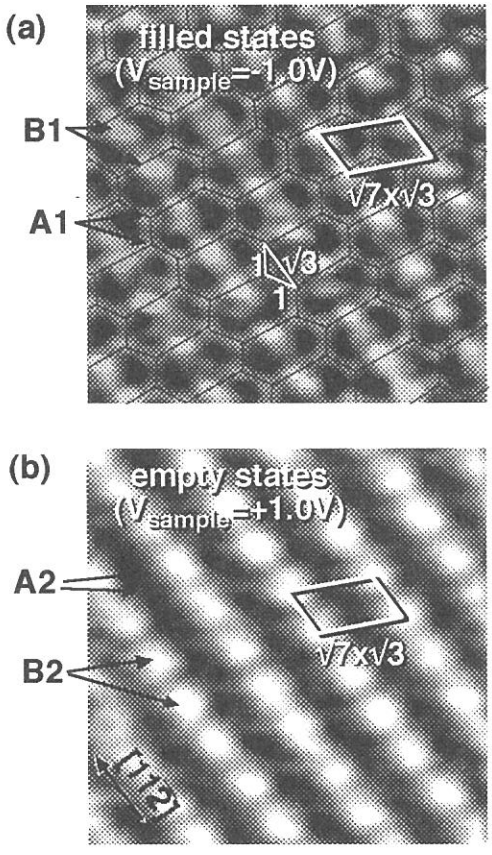

Fig.1 Images of filled states (a) and empty states (b) for the Si(111) $\sqrt{7}\times\sqrt{3}$-(Pb, Sn) surface.

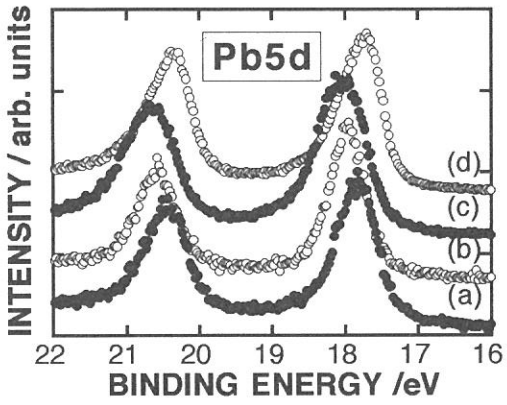

Fig.2 Pb 5*d* photoelectron spectra of Si(111) $\sqrt{7}\times\sqrt{3}$-(Pb, Sn) surface (a), Si(111) $\sqrt{3}\times\sqrt{3}$-Pb surface with 1/6 ML Pb coverage (b), Si(111) $\sqrt{3}\times\sqrt{3}$-Pb surface with 1/3 ML Pb coverage (c), and Si(111) 1×1-Pb surface with 1 ML Pb coverage (d). Intensities of the spectra are normalized at the peaks of the j=5/2 lines.

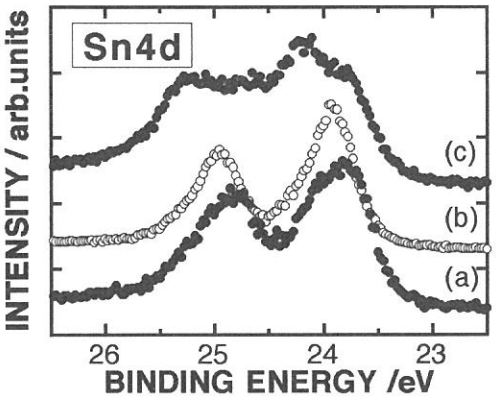

Fig.3 Sn 4*d* photoelectron spectra of Si(111) $\sqrt{7}\times\sqrt{3}$-(Pb, Sn) surface (a), Si(111) $2\sqrt{3}\times2\sqrt{3}$-Sn surface with 1 ML Sn coverage (b), and Si(111) $\sqrt{3}\times\sqrt{3}$-Sn surface with 1/3 ML Sn coverage (c). Intensities of the spectra are normalized at these maxima.

adsorbate system with various coverages of Pb and Sn, respectively. The Pb 5*d* spectrum for the Si(111) $\sqrt{7}\times\sqrt{3}$-(Pb, Sn) surface shows tailing towards the high binding energy side, compared with that for the Si(111) $\sqrt{3}\times\sqrt{3}$-Pb surface with 1/6 ML Pb coverage, where Pb and Si adatoms in T_4 sites form a semiconducting surface [4]. The observed tailing is attributed to metallic nature of the surface, although it is not so extended as the Si(111) 1×1-Pb surface, where about 1 ML Pb is considered to form a metallic layer [5,6]. On the other hand, the Sn 4*d* spectrum exhibits two major components for the Si(111) $\sqrt{3}\times\sqrt{3}$-Sn surface, as reported so far [7,8], and single component for a bulklike α-Sn structure on the Si(111) $2\sqrt{3}\times2\sqrt{3}$-Sn surface [9]. For the Si(111) $\sqrt{7}\times\sqrt{3}$-(Pb, Sn) surface, the Sn 4*d* spectrum also shows shoulder structures at the high binding energy side of the main peaks. This definitely indicates at least two different Sn-Si bonds or inequivalent Sn adsorbing sites on the Si(111) $\sqrt{7}\times\sqrt{3}$-(Pb, Sn) surface. Thus, we ascribe the bright spots at the T_1 site (A) and those at the T_1 and H_3 sites (B) in the STM images to Pb and Sn adatoms, respectively. The present results lend support to a proposed model for the atomic arrangement of the Si(111) $\sqrt{7}\times\sqrt{3}$-(Pb, Sn) surface [3].

References

[1] J. Yuhara, R. Ishigami, K. Morita, Surf. Sci. **326** (1995) 133.

[2] D. Nakamura, J. Yuhara, K. Morita, Appl. Surf. Sci. **130/132** (1998) 72.

[3] J. Yuhara, D. Nakamura, K. Soda, K. Morita, Surf. Sci., *in press*.

[4] C.J. Karlsson, E. Landmark, Y.-C. Chao, and R.I.G. Uhrberg, Phys. Rev. **B**45 (1992) 6321.

[5] J.A. Carlisle, T. Miller, and T.-C. Chiang, Phys. Rev. **B**45 (1992) 3400.

[6] X. Tong, K. Horikoshi, and S. Hasegawa, Phys. Rev. B**60** (1999) 5653.

[7] M. Göthelid, M. Björkqvist, T.M. Grehk, G. Le Lay, and U.O. Karlsson, Phys. Rev. **B**52 (1995) R14352.

[8] R.I.G. Uhrberg, H.M. Zhang, T. Balasubramanian, S.T. Jemander, N. Lin, and G.V. Hansson, Phys. Rev. **B**45 (2000) 8082.

[9] A.H. Levermann, P.B. Howes, K.A. Edwards, H.T. Anyele, C.C. Matthai, J.E. Macdonald, R. Feidenhans'l, L. Lottermoser, L. Seehofer, G. Falkenberg, and R.L. Johnson, Appl. Surf. Sci. **104/105** (1996) 124.

BL5A: Cesiumoxide-GaAs Interface and layer thickness in NEA surface formation

Sam D. Moré [1], Senku Tanaka [2], Shin-ichiro Tanaka [1*], Tomohiro Nishitani [3], Tsutomu Nakanishi [3] and Masao Kamada [1, 2]

[1] *UVSOR Facility, Institute for Molecular Science, Okazaki 444-8585, Japan*
[2] *Department of Structural Molecular Science, The Graduate University for Advanced Studies, Okazaki 444-8585, Japan*
[3] *Department of Physics, Nagoya University, Nagoya 464-8602, Japan*

Negative electron affinity (NEA) surfaces have found applications as efficient photocathodes and the NEA surface of GaAs(100) and its superlattice is known to be a useful emitter of spin-polarized electrons with a high degree of polarization and efficiency. This can be achieved by the 'jo-jo'-technique, where Cs deposition and subsequent oxidation are repeated several times. The details of NEA surface formation, however, are not fully understood: previous reports [2-4] differ considerably both in describing the method of production as well as the underlying chemical and physical mechanism.

Fig. 1 shows the electron yield as a function of sample treatment. Curve (a) shows Cs deposition only. Curve (b) shows the so called Nagoya treatment; Cs is dosed until the electron yield decreases again, the yield raises under O expose. Curve (c) depicts the classical jo-jo treatment; the GaAs surface is alternately exposed to Cs and O, O lowers the electron yield, while Cs increases it. Curve (d) shows a mixed type of activation where during the initial Cs deposition small amounts of O have been added. This treatment involves larger Cs and O amounts. It is characteristic for saturation regimes of both O and Cs, resulting in the generation of overlayers with a larger thickness.

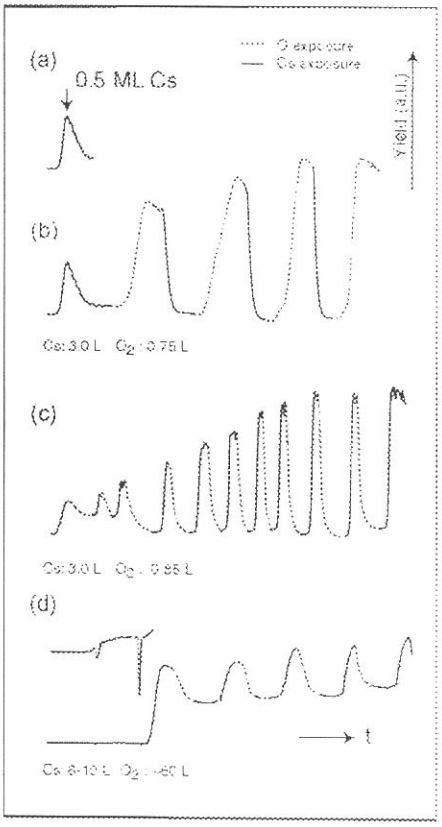

FIGURE 1. Electron yield as a function of sample treatment for different activation processes on GaAs(100): (a) Cs-only activation, (b) so-called Nagoya treatment, (c) classical jo-jo treatment, and (d) a mixed type of activation.

Fig. 2 shows the Ga-3d and As-3d photoemission spectra after the activation. All activations can achieve a high electron yield. The stability of the yield is however different with Phase III activations being frequently less stable than Phase I and Phase II activations. The As-3d peak for Phase I is broadened towards higher kinetic energy, indicating donation of electrons by reaction with Cs. In Phase II the As-3d peak has split into a larger main peak and a smaller peak at 53-54 eV (47-46 eV binding energy), which marks the As=O double bond formation. The broadening to the higher kinetic

energy side is less pronounced. This indicates that Phase II has a larger interface oxidation at the As than Phase I.

Phase III finally shows a strong interface oxidation. The direct Cs-interaction with the substrate seems to be negligible. The Ga and As core-level peaks for Phase III are much broader than the peaks of the previous phases. Also the halfwidth of the Cs-peak is about 25% broader. This indicates that the Cs in this phase consists of more different ionization stages than the one of Phase I. The chemical composition of the thicker overlayer is far more complex and heterogeneous than for the Phases I and II. The lower stability in terms of electron yield for the Phase III surface could be due to an ongoing chemical reaction inside such an overlayer.

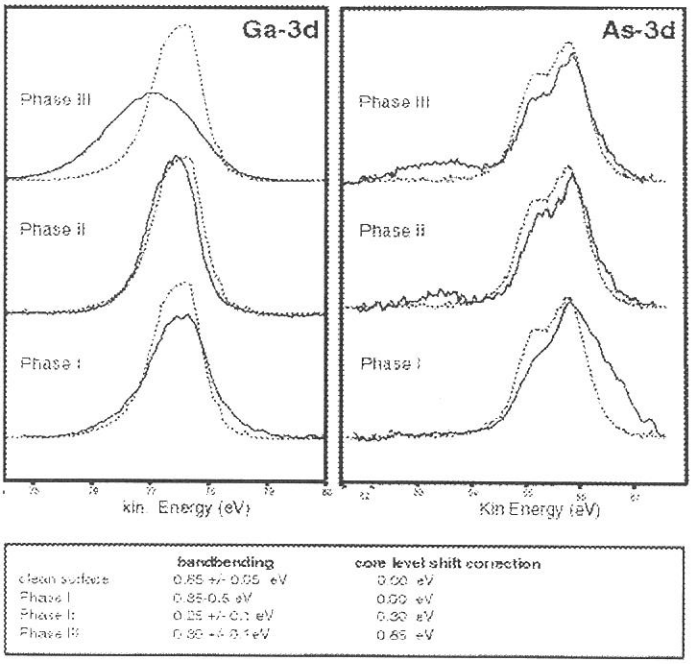

FIGURE 2 Ga-3d and As-3d core-levels representative for different activation processes. Peak positions are corrected for bandbending. The dotted line shows the clean surface. Phase I corresponds to the activation (b), Phase II to the activation (c) and Phase III to the activation (d).

The Table below Fig. 2 gives the bandbending values obtained from the surface photovoltage experiment, which the photoemission data have been corrected for. A stronger oxidation of As is correlated with a decrease in bandbending in our experiment, which is in alignment with previous results from literature [2,3]. The Table shows a decrease in bandbending from Phase I to Phase III. None of the surfaces investigated in our study has shown therefore any increase in bandbending. This contrasts the dipole model as originally proposed [2].

Summarizing, three different NEA activation processes on GaAs(100) have been characterized using high resolution photoemission spectroscopy. Analyzing the influence of the cesiation and oxidation on the bandbending and monitoring the electron yield from bulk GaAs(100), we have been able to distinguish three different phases of activation, which depend on the total thickness of the overlayer, the Cs:O ratio and the resulting chemical interaction with the substrate.

References

1. C.Y. Su, W.E. Spiecer and I. Lindau, *J. Appl. Phys.* **54** (1983) 1413.
2. A. Alperovich, A.G. Paulish, A.S. Terekov, *Surf. Sci.* **331-333** (1995) 1250-1255.
3. M. Besancon, R. Landers and J. Juille, *J. Vac. Sci. Techn.* **A5** (1987) 2025.
4. N. Takahashi, S. Tanaka, M. Ichikawa, Y. Cai and M. Kamada, *J. Phys. Soc. Japan* **66** (1997) 2798.

(BL 5A)

Surface photo-voltage effects on GaAs-GaAsP superlattices studied with combination of SR and laser

Senku Tanaka,[1] Sam D. Moré,[2] Kazutoshi Takahashi,[2] Tomohiro Nishitani,[3] Tsutomu Nakanishi [3] and Masao Kamada [1, 2]

[1] *Department of Structural Molecular Science, The Graduate University for Advanced Studies, Okazaki 444-8585*

[2] *UVSOR Facility, Institute for Molecular Science, Okazaki 444-8585*

[3] *Department of Physics, Nagoya University, Nagoya 464-8602*

Electronic non-equilibrium in the surface layers of photo-excited semiconductors has been attracting much interest from the basic scientific point of view and also from the field of practical applications of photo devices. Many works have been carried out by means of electrical methods using various types of contacting electrodes, but few works have so far been reported on transient non-equilibrium in the interface between semiconductor surfaces and the vacuum. GaAs is one of the most useful semiconducting materials. Especially the negative-electron affinity (NEA) surface of a *p*-type GaAs (100) can provide spin-polarized electrons when it is excited with circularly polarized light. The NEA surface is produced by the so-called yo-yo technique, where cesium and oxygen are deposited repeatedly on clean *p*-GaAs (100) surfaces. It has been pointed out that the electron density saturates when semiconductor photo-cathodes are excited with intense pulsed lasers. Gometz *et al.*[1] have proposed that the surface photo-voltage (SPV) effect plays an important role to cause the saturation and that a metallic overlayer may be useful to prevent the effect from interfering in future high-energy experiments. The use of superlattice photo-cathode as a polarized electron source has been suggested by Togawa *et al.*,[2] since the transport of photo-carriers is expected to be well suppressed in the superlattice system. The SPV effect of superlattice system is therefore of both technical and theoretical interest.

In the present work, the SPV effect on GaAs-GaAsP superlattices has been investigated by using core-level photoelectron spectroscopy with the combination of SR and laser. The schematic energy diagram is shown in Fig. 1. This kind of photoelectron spectroscopy can provide information on the electronic structures in a wide energy range for photo-excited semiconductor surfaces. The core-level photoelectron spectroscopy is more surface-sensitive in comparison with others using

laser and a Kelvin method, since the escape depth of electrons has a minimum around 30-100 eV in kinetic energy. The energy shift of the core-level photoelectron spectra can give us the reliable SPV values as shown in Fig. 1.

The Ga-3*d* photoelectron spectra showed transient energy shifts due to the SPV effect at low temperatures, but not at room temperature. The amount of the SPV effect was about 50 meV, which is very much smaller than that of clean GaAs (100) surfaces. The present result is in good agreement with the proposal by Togawa et al., but the existence of the small amounts of SPV effects even at low temperatures indicates that another mechanism is required in order to suppress the SPV effect completely at any temperature.

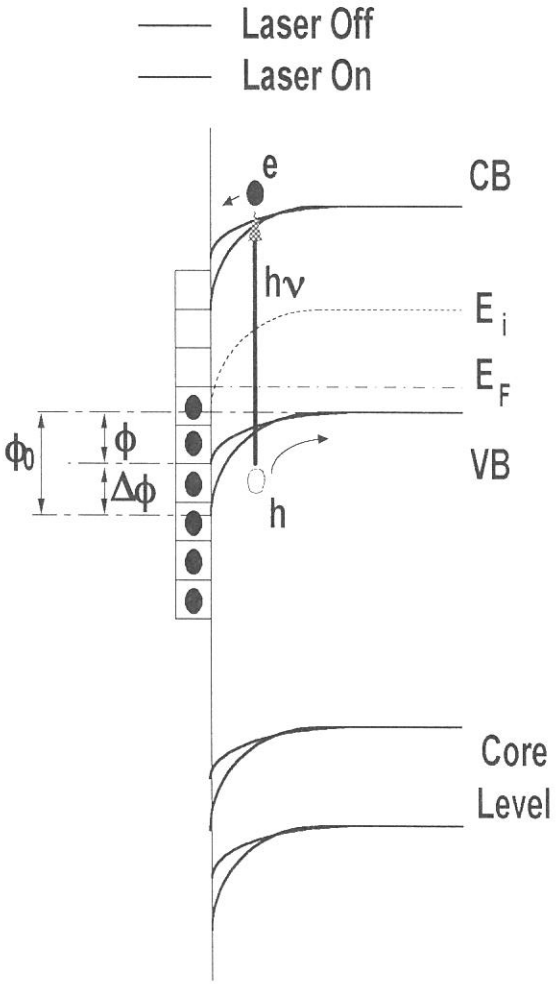

Fig. 1. Schematic diagram of SPV effect

The NEA surface of the superlattice was also prepared by a so-called yo-yo technique. The SPV effects were observed on these NEA surfaces of GaAs (100) and GaAs-GaAsP superlattice, but the amounts of the SPV effect on NEA surface of the superlattice was so small (about 10 meV) in comparison with that of the GaAs.

In conclusion, The SPV effect has been investigated on GaAs-GaAsP superlattices using core-level photoelectron spectroscopy with combination of SR and laser. It was observed that the SPV effects are so small on the clean and NEA surfaces of the superlattice, in comparison with those of bulk GaAs.

References

1) A. Herrera-Gomez, G. Vergara, and W. E. Spicer, J. Appl. Phys. 79, 7318 (1996).

2) K. Togawa, T. Nakanishi, T. Baba, F. Furuta, H. Horinaka, T. Ida, Y. Kurihara, H. Matsumoto, T. Matsuyama, M. Mizuta, S. Okumi, T. Omori, C. Suzuki, Y. Takeuchi, K. Wada, K. Wada, and M. Yoshioka, Nucl. Instrm. Methods A 414, 431 (1998).

(BL 5A)

Time-dependence of the surface photovoltage effect on GaAs (100) studied with combination of SR and laser: Microsecond time-response

Senku Tanaka[A], Kazutoshi Takahashi[B], Sam D Moré[B], and Masao Kamada[A, B]

[A] *The Graduate University for Advanced Studies, Myodaiji, Okazaki, 444-8585*
[B] *UVSOR Facility, Institute for Molecular Science, Myodaiji, Okazaki, 444-8585*

Electronic non-equilibrium in the surface layers of photo-excited semiconductors has been attracting much interest from the basic scientific point of view and also from the field of practical applications of photo devices. Many works have been carried out by means of electrical methods using various types of contacting electrodes, but few works have so far been reported on transient non-equilibrium in the interface between semiconductor surfaces and the vacuum. Photoelectron spectroscopy is one of the most powerful tools to investigate surface electronic properties because of the very short escape depth of photoelectrons. Recently, we have studied photo-induced change in GaAs (100) surface using core-level photoelectron spectroscopy with synchrotron radiation and laser [1], since photoelectron spectroscopy is one of the most powerful tools to investigate surface electronic properties because of the very short escape depth of photoelectrons. It has been observed that the laser-induced core-level shift is caused by the surface photovoltage (SPV) effect. And it has been also found that there are at least two components in the recover process of the SPV. In this report, we present the time response of the SPV effect on GaAs (100).

Experiments have been conducted at BL5A, UVSOR facility. We used the laser (COHERENT Mira 900-F (90 MHz, 800 nm) & RegA (10 KHz, 800 nm)) as the excited light source to cause the SPV effect in the nano-second and micro-second time-domains, respectively. The laser light was transported to the view-port of the measurement chamber using an optical fiber and focused on the sample surface. The OMICRON electron-energy analyzer (EA-125HR) was used to observe the photoelectron spectra. The single signal from the analyzer was used for time-dependent measurements although the analyzer has five channel detectors. Photoelectron signals from the electron analyzer were changed to LED signals in the pre-amplifier circuit in order to decrease the electric noises. Photoelectron signals were transferred to the gate circuit, which was controlled as well as the mechanical shutter. The photoelectron signal was used as a start signal for a time-to amplitude converter (TAC). Laser pulse was monitored by a PIN photodiode, and was used as a stop signal. A couple of TACs has been used, corresponding to the signals with and without laser excitation. By using this system, it is possible to observe the time dependence of photoelectron signals at a fixed kinetic energy. In the present study, it has been observed that the SPV effect caused by the laser excitation decays in the microsecond range as discussed below.

Figure 1 (a) shows Ga-3d core-level photoelectron spectra of GaAs (100). Solid and dotted lines represent Ga-3d spectra with and without laser irradiation, respectively. It is clearly observed that the Ga-3d core-level shifts to the higher kinetic-energy side under irradiation of the laser. This shift originates from the SPV effect caused by the laser-excited photocarriers. Figure 1 (b) represents the time response of the photoelectron intensity at 77.9 eV and 78.8 eV, respectively. It should be noted that there are at least two components in the response curve of the photoelectron intensity; one is the fast component time constant of about 1μs and another has a larger constant of about 13μs. They are attributed to the surface and bulk origin, respectively, since the fast component was not observed on the negative-electron affinity surfaces.

In summary, we have investigated the time-dependence of the SPV effect on GaAs (100) in microsecond region. It has been observed that there are at least two components in the recover process of the SPV effect in microsecond region.

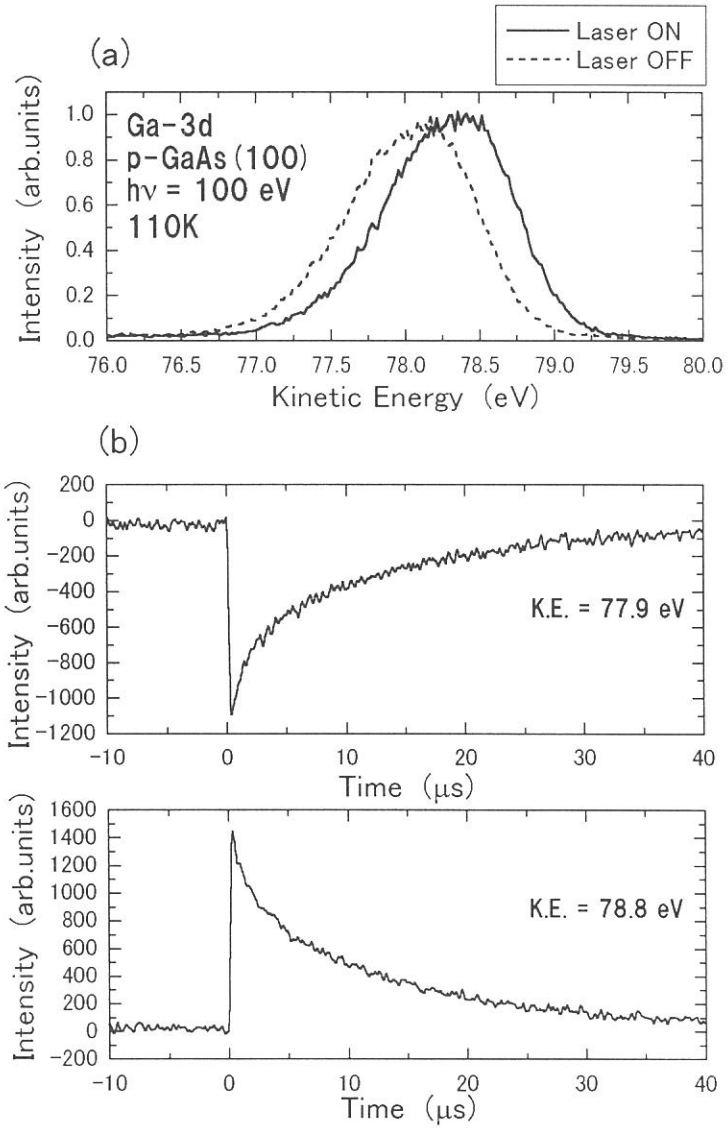

Figure 1. (a) Ga-3d photoelectron spectra of GaAs (100). Solid and dotted lines represent Ga-3d spectra with and without laser excitation, respectively. (b) Temporal profiles of the photoelectron intensity at 77.9 eV and 78.8 eV, respectively.

References

[1] M. Kamada et al., *Surf. Sci.*, **454-456** (2000) 525.

(BL-5B&6A2)

Photoemission Study on the Surface Photovoltage For Si(111) Surface Induced by Laser Light Irradiation

Yuichi Haruyama[A], Taichi Okuda[B], Ayumi Harasawa[B], Toyohiko Kinoshita[B], Shin-ichiro Tanaka[C], Hideo Makino[D], Katsuo Wada[D], Kazutoshi Fukui[E], Masao Kamada[E] and Shinji Matsui[A]

[A]*LASTI, Himeji Institute of Technology, 3-1-2 Kouto, Kamigori, Ako 678-1205, Japan*
[B]*Synchrotron Radiation Laboratory, Institute for Solid State Physics, University of Tokyo, Kashiwa 277-8581, Japan*
[C]*Faculty of Science, Nagoya University, Furo-cho, Chikusa-ku, Nagoya 464-8602, Japan*
[D]*Silicon Technology LTD, 897-20 Kyowa, Mochizuki, Kitasaku-gun, Nagano 384-2204, Japan*
[E]*Institute for Molecular Science, Okazaki 444-8585, Japan*

Recently, the research on the surface photovoltage (SPV) has been performed at super-ACO in France using the FEL light [1]. In the study, it was observed that the band bending is decreased when the synchronized FEL light and SR are irradiated for Si(111) 2x1 and GaAs-Ag surface. At UVSOR, SPV for GaAs surface was also observed using synchronized laser light and SR [2]. In addition, we observed SPV for Si(111) surface using CW laser light irradiation [3]. In these cases, SPV is induced to decrease the band bending between semiconductiong surface and bulk. The mechanism of SPV is explained by a model that the carrier induced by laser light irradiation transfers to the surface. However, it is not clear whether SPV is associated with the surface state. Moreover, it is not clear whether the same senario is applied in the case of the metallic surface or in the case of the semiconducting surface. In order to investigate the relationship between SPV and the surface state, between SPV and the carrier concentration, we have performed the combined study of the photoemission and laser light irradiation.

The experimental setup including the optical alignment was described by Ref. 3 in detail. Photoemission experiments were carried out by using a conventional UHV system (FISONS, ESCALAB-220i-XL) at a base pressure of 2×10^{-8} Pa [4]. Total instrumental energy resolution at room temperature was 0.3~0.5 eV full width at half maximum, depending on the photon energy ($h\nu$) in the energy range of 50~130 eV. Photoemission experiments were also performed with higher energy resolution of ~0.1 eV at PF. The clean surface was obtained by annealing the sample at ~1200°C using the laser light irradiation ($h\nu$ = 1.165 eV) and checked by x-ray photoemission spectroscopy and LEED. The temperature of the sample was measured with an optical pyrometer.

Figure 1(a) and (b) show the Si 2*p* core-level photoemission spectra (closed dots) for n- (P-dope, 9-14Ω) and p-type (B-dope, 10-20 Ω) Si (111) surface at 90K, respectively. Under the laser light irradiation, the photoemission spectra (open dots) for the n-type (p-type) Si(111) surface shift to higher (lower) binding energy side. The shift direction for the n- and p-type Si(111) surface was opposite. It is considered that the observed rigid shift is caused by SPV induced by the laser light irradiation.

Figure 2 shows the impurity (carrier) concentration dependence of SPV obtained by the photoemission spectra. With increasing the impurity concentration, SPV is increased (decreased) for n-type (p-type) Si(111) surface. The shift is associated with the band bending because the band bending is increased with the impurity concentration. However, for the higher doping concentration, the shift was not observed in our measurements.

Figure 3 shows the valence band photoemission spectrum for $\sqrt{3}x\sqrt{3}$ Si (111)-Bi surface (n-type, P-dope 9-14 Ω) at room temperature. For the $\sqrt{3}x\sqrt{3}$ Si (111)-Bi surface, it is known that the surface state near the Fermi level disappears and the band gap is open. Under the laser light irradiation, the photoemission spectrum for the $\sqrt{3}x\sqrt{3}$ Si (111)-Bi surface shifts to higher binding energy side by ~0.2 eV. The shift is identical to that for the clean 7x7 Si(111) surface. This means that SPV is not associated with the surface state in this system.

References

[1] M. Marusi, L. Nahon, D. Garzella, T. Hara, R. Bakker, M. Billardon, A. Delboulbe, G. Indlekofer, and A. Taleb-Ibrahimi, Appl. Phys. Lett. **70** (1997) 895.

[2] M. Kamada, S. Asaka, T. Tsujibayashi, O. Arimoto, M. Watanabe, S. Nakanishi, H. Itho, S. Hirose, and M. Itho, J. Jpn. Soc. for Synchrotron Radiation Research **12** (1999) 48.

[3] Y. Haruyama , T. Kinoshita, S. Tanaka, H. Makino, and S. Matsui, UVSOR Activity Report 1999, p.128.

[4] T. Kinoshita, K. G. Nath, Y. Haruyama, M. Watanabe, S. Yagi, S. Kimura, and A. Fanelsa, J. Electron Spectrosc. Relat. Phenom. **92**(1998)165.

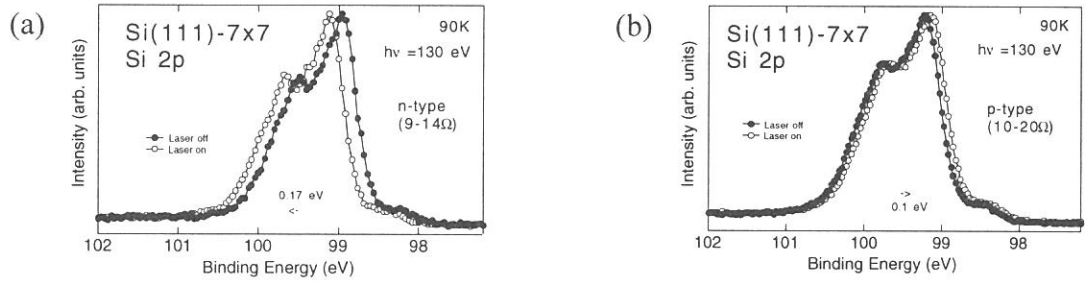

Fig. 1 Si 2*p* core-level photoemission spectrum (a) for the n- and (b) p-type Si(111) surface with laser light irradiation (open dots) and without laser light irradiation (closed dots).

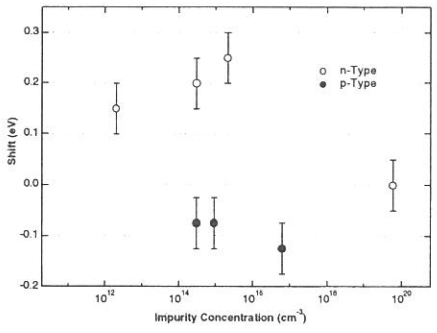

Fig. 2 Impurity concentration dependence of SPV for n- (open dots) and p-type (closed dots) Si (111) surfaces.

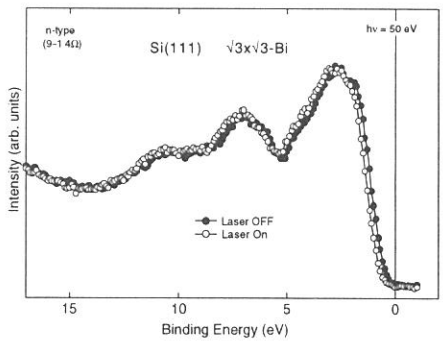

Fig. 3 Valence band photoemission spectrum for Si(111) $\sqrt{3}x\sqrt{3}$-Bi surface with laser light irradiation (open dots) and without laser light irradiation (closed dots).

(BL6A2)

Photoelectron spectroscopic study on photo-induced phase transition in a spin crossover complex $Fe(2\text{-pic})_3)Cl_2EtOH$

Masao Kamada, Yoichiro Doi, [A] Kazutoshi Fukui, [B] Yuichi Haruyama, [C] Takeshi Tayagaki, [E] Naoki Yonemura, [E] and Kouichiro Tanaka [E]

UVSOR Facility, Institute for Molecular Science, Okazaki 444-8585
[A] *College of Engineering, Fukui University, Fukui 910-8507*
[B] *VUV-PhotoScience, Institute for Molecular Science, Okazaki 444-8585*
[C] *LASTI, Himeji University, Hyogo 678-1201*
[E] *Faculty of Science, Kyoto University, Kyoto606-8502*

In recent years, photon-induced phenomena attract much interest. For examples, photon excitation changes the crystal structures, magnetic and optical properties, and so on. These new phenomena are called as photo-induced phase transitions, which are expected to produce new properties of condensed matters.

In order to investigate the photo-induced phase transitions, optical spectroscopic techniques such as optical absorption and reflection have been mostly used, since these techniques can monitor the phenomena in a fast time domain and are easily obtained. However, these techniques have some limitation. For examples, only narrow energy range in the valence electrons can be observed by the optical spectra. The purpose of the present study is to investigate the photo-induced effects on electronic states in wide energy range using photoelectron spectroscopy. We have been developing new techniques based on the combination of synchrotron radiation and laser in recent years. We have applied this technique to the present purpose.

Experiments have been carried out at beam lines BL5B and BL6A2, where a plane-grating monochromator provides photons in a wide energy range from UV to EUV. A VG-microESCA system consisting of XPS and UPS components was used to obtain the photoelectron spectra. A single crystal of $[Fe(2\text{-pic})_3]\ Cl_2EtOH$ was grown at Kyoto university and was filed in a preparation chamber. The sample was attached on the holder of a flow-type He cryostat and was cooled down to about 40 K. The cw Ar^+ laser light was introduced in an analyzing chamber. The sample changed its color from yellow to red and from red to yellow by cooling and photo-excitation, respectively.

Figure 1 shows UPS spectra of valence states of $Fe(2\text{-pic})_3]\ Cl_2EtOH$. The spectra observed at room temperature did not show any change by laser excitation, but it should be noted that the valence states drastically changed by cooling the

sample from RT to 40K and also by the laser-excitation at 40K.

It has been believed from the optical spectroscopic studies that $Fe(2\text{-pic})_3]Cl_2EtOH$ shows high-spin and low-spin states in Fe ions at RT and low temperatures, respectively, and that the low-spin state (low-temperature phase) is changed by photo-excitation to the high-spin state (high-temperature phase). However, the present experimental results indicate that the photo-induced phase transition of $Fe(2\text{-pic})_3]Cl_2EtOH$ is not the same as the high-spin state, where the Fe-3d state may play an important role to trigger the photo-induced phase transition.

Fig. 1. Photoelectron spectra of $Fe(2\text{-pic})_3]Cl_2EtOH$ at RT and 40 K with and witout laser excitation.

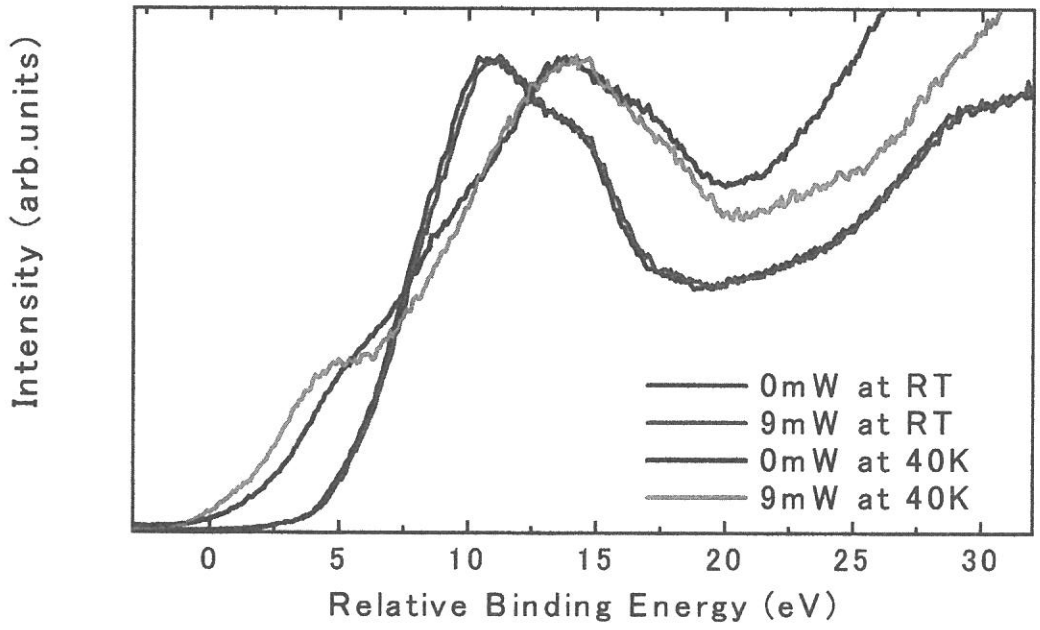

at RT at 40 K with laser at 40 K

(BL6A2)

Comparison of Auger-Free Luminescence and Valence-Band Photoemission in CsCl, CsBr and BaF_2

M. ITOH, M. KAMADA[1] and K. SAWADA

Faculty of Engineering, Shinshu University, Nagano 380-8553

[1] *UVSOR Facility, Institute for Molecular Science, Okazaki 444-8585*

Auger-free luminescence (AFL) has attracted a lot of particular interest in both fundamental and applied research ever since it was discovered in 1983. In the present work, we have studied the line shape of AFL in CsCl, CsBr and BaF_2 in comparison to the data of ultraviolet photoelectron spectroscopy (UPS) of the valence band. The lattice relaxation effect on AFL will be discussed in brief.

A thin film sample was fabricated *in-situ* by evaporation on a gold substrate in a preparation chamber, and was then transferred into an analyzing chamber. The starting materials were crystal ingots obtained from the Horiba Company. Thickness of the specimens was maintained at about 100 Å. Measurements of the luminescence and photoemission spectra were both carried out for the same samples in an identical analyzing chamber to eliminate any uncertainty due to sample preparation. The base pressure in the analyzing chamber was better than 2×10^{-8} Pa during the measurements.

The UPS spectra were measured at 295 K by using an angle-resolved hemispherical analyzer under the multi-bunch operation of SR, with a resolution of 0.21–0.23 eV. On the other hand, the AFL spectra were measured at 295 and 90 K by using a time-resolved detection technique under the single-bunch operation of SR, with a resolution of 0.15–0.20 eV. The obtained luminescence spectra were corrected for the spectral response of the detection system, and were given in arbitrary units of photon numbers per unit energy.

Figure 1 shows UPS spectrum of CsCl excited with 24.7-eV photons. A low-energy band at 7.0 eV is apparently due to the j = 3/2 component of the spin-orbit-split Cs^+ 5*p* levels. A single band at 12.7 eV is referred to the valence band associated with the Cl^- 3*p* states. One may see a weak tail-like structure on the high-kinetic-energy side of the valence band. This signal arises from the gold substrate, indicating that our evaporated film is thin enough to neglect the charging effects. For a direct comparison to the AFL spectrum, the valence-band UPS spectrum has to be replotted relative to the maximum of the Cs^+ 5*p* core band. After the Cs^+ 5*p* band was deconvoluted with a Gaussian instrumental resolution profile, the edge energy was determined as a characteristic energy at which the photoemission intensity decreases to the 1/10 value of the peak intensity. The maximum energy was thus obtained to be 7.86 ± 0.10 eV in Fig. 1.

The AFL spectrum of CsCl measured at 295 K under the excitation with 25.0-eV photons is presented by solid curve in Fig. 2. The result is essentially the same as that of bulk CsCl [1]. The valence-band UPS spectrum replotted relative to the maximum of the core band is also shown by open circles in Fig. 2, where the background structure due to gold substrate has been subtracted from the spectrum. Both curves are normalized to unity at their maxima.

The valence-band UPS spectra of CsBr and BaF_2, replotted relative to the maximum of the core band, are shown by open circles in Figs. 3 and 4, respectively. The AFL of CsBr was stimulated at 295 K with

use of the zero-order SR transmitted through an aluminum filter (transmits radiation between about 16 and 70 eV), while the 90-K AFL spectrum was excited with monochromatized SR at 25.0 eV. These results are depicted by deep and light solid curves in Fig. 3. The solid curve in Fig. 4 shows AFL spectrum of BaF_2 stimulated with 25.0-eV photons at 295 K. The high-energy spectrum above 6.5 eV was reproduced from the data obtained in Ref. [2].

The present results of Figs. 2 - 4 have some common features, which are summarized as follows: (1) The main band of AFL is situated at the bottom of the valence band. (2) The low-energy tail of AFL exists outside of the valence band. (3) The total width of AFL is somewhat narrower than that of the valence band. These facts are explained on the basis of the lattice relaxation model. According to this model, when a hole is generated in the core band, it quickly relaxes into a self-trapped state and deforms the lattice configuration in its immediate vicinity. Because of the Franck-Condon principle, such a deformation is kept well during the radiative transition, leading to the above-mentioned facts (1), (2) and (3).

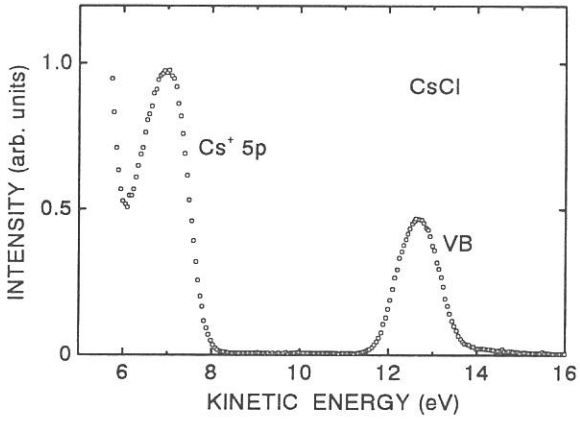

Fig. 1. UPS spectrum of CsCl excited with 24.7-eV photons.

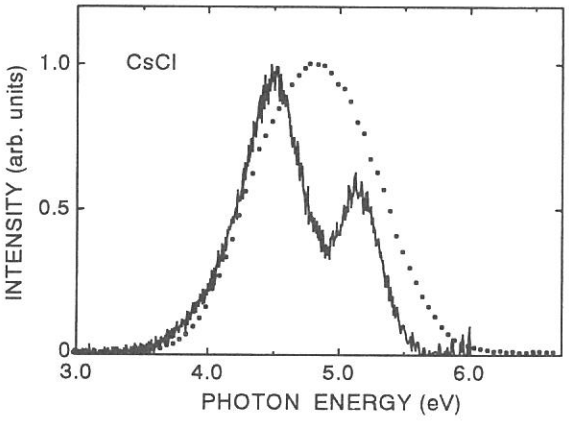

Fig. 2. Comparison of AFL (solid curve) and valence-band UPS (open circles) spectra of CsCl.

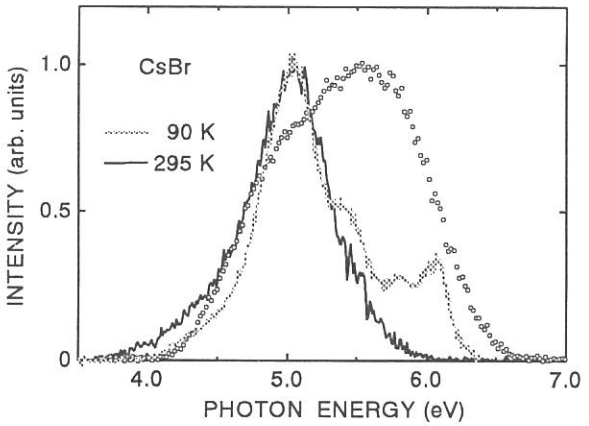

Fig. 3. Comparison of AFL (solid curves) and valence-band UPS (open circles) spectra of CsBr.

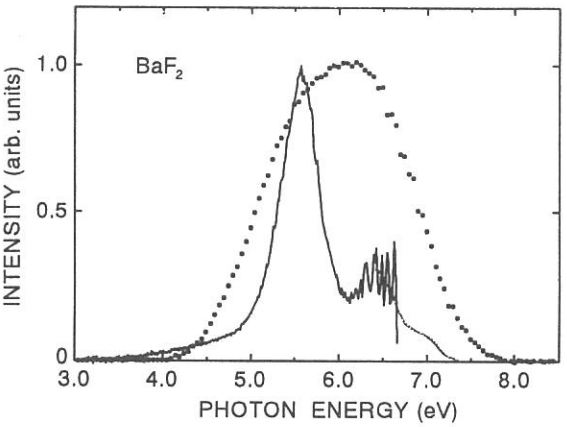

Fig. 4. Comparison of AFL (solid curve) and valence-band UPS (open circles) spectra of BaF_2.

[1] M. Itoh, M. Kamada and N. Ohno : J. Phys. Soc. Jpn. **66** (1997) 2502.

[2] J. L. Jansons, V. J. Krumins, Z. A. Rachko and J. A. Valbis : Phys. Status Solidi B **144** (1987) 835.

(BL7A)

XANES analysis of Cu-MgO/TiO_2 bactericidal material

Tomomi Kosaka, Ayano Yamada, Atsuyuki Miyaji, Mayumi Shiraishi, Sadao Hasegawa

Department of Chemistry, Tokyo Gakugei University, Koganei, Tokyo, 184-8501

TiO_2 was well known for its photocatalytic function such as NOx reduction[1], self-cleaning[2], super-hydrophilic[3]...etc. However, the effects were specifically weakened without UV radiation. Therefore, the noble metal loaded TiO_2 was utilized for keeping its activity even if in the dark place.

Recently, food poisoning was occurred by the water contamination with *O-157 Esherichia coli*, *Staphylococus aureus* and so on. Then, much attention was given to the bactericidal ceramics and the technology of water purification using the materials. It was known that MgO, one of basic catalyst, had the bactericidal function when it involved in the polluted water at higher concentration. However, the mechanism of bactericidal effects was not so clear.

In this report, we prepared MgO/TiO_2 and Cu-MgO/TiO_2 catalysis, investigated that crystal structure and chemical condition of the sample surface from the results of Mg K-edge XAFS analysis.

MgO/TiO_2 and Cu-MgO/TiO_2 catalysis were prepared by the impregnation method and the concentration of MgO was 25wt% in the both samples. They were calcined at 873, 1073, 1273K for 3h in air.

Mg K-edge XAFS measurement was carried out on the BL-7A at UVSOR, Institute for Molecular Science, Okazaki, Japan. The storage ring was operating at electron energy of 750MeV. The spectra were recorded in a total electron yield mode under high vacuum ($<3x10^{-7}$) at room temperature. Data were collected using $KTiPO_4$ [KTP] (011) double crystal monochromator. The samples were put on the first Cu-Be dynode of the electron multiplier using adhesive carbon tape.

Fig.1 were shown Mg K-edge XANES spectra of MgO/TiO_2 samples calcined at various temperatures. Fig.2 were also shown Mg K-edge XANES spectra of some reference samples. The spectra of MgO/TiO_2 calcined over 873K were corresponding to that of $MgTiO_3$. It was indicated that solid phase reaction was occurred between MgO and TiO_2 over 873K. Mg K-edge XANES spectra of Cu-MgO/TiO_2 samples were also shown in Fig.3. In the case of Cu-MgO/TiO_2 samples, the spectra were varied with the calcinations temperature. The spectra at 873K and 1073K were resembled to that of MgO, oxygen atoms in this sample hexagonally surrounded Mg atoms. On the other hand, the change of Mg environmental structure was occurred at 1273K, the resulting coordination number of Mg atoms was 12 (perovskite structure) on the surface. However, the difference of the surface structure due to Cu atom addition was not clarified in this analysis.

The bactericidal effects to *Esherichia coli (IFO 3972)* of these samples were investigated in progress. However, the Mg addition was certainly enhanced the bactericidal function of TiO_2.

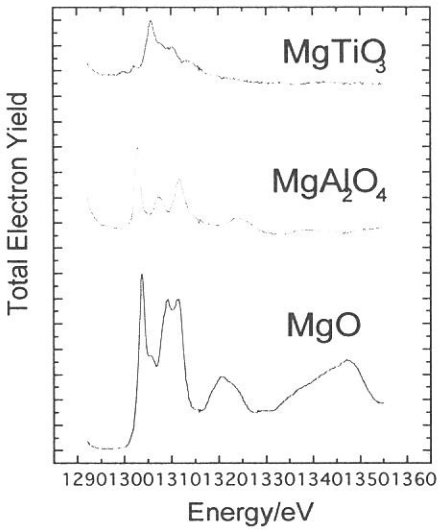

Fig.1 Mg K-edge XANES spectra of Reference samples

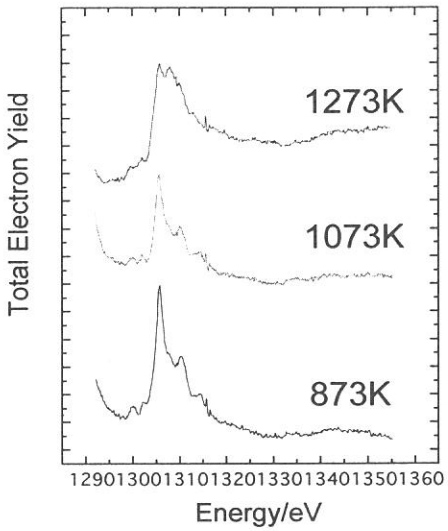

Fig.2 Mg K-edge XANES spectra of 25wt% MgO/Ti_2O

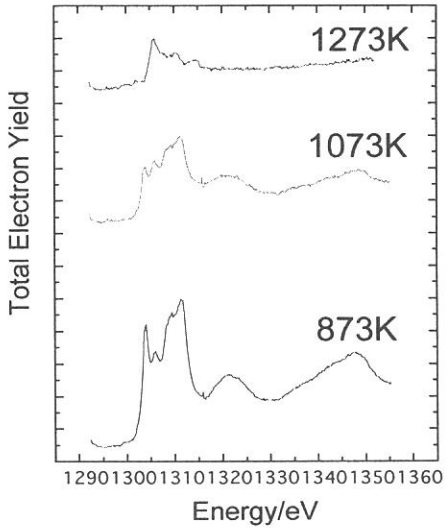

Fig.3 Mg K-edge XANES spectra of Cu-MgO/Ti_2O

1) K. Takeuchi, *Kagaku to Kogyo*, **46**(12), 1839(1993).

2) A. Ishizaki, *Hyomen Gijyutu*, **50**(3), 251(1999).

3) R.Wang et al., *Nature*, **338**, 431(1997)

(BL7A)

Mo L_{III}-edge XANES Study of Molybdena on Silica-Alumina in Contact with Propene

Hirofumi Aritani[a]*, Osamu Fukuda[a], Noboru Tanida[a], Tatsuya Yamamoto[a],
Masato Tamai[a], Atsushi Nakahira[a], Atsuyuki Miyaji[b], and Sadao Hasegawa[b]
[a]*Faculty of Engineering and Design, Kyoto Institute of Technology, Sakyo-ku, Kyoto 606-8585*
[b]*Department of Chemistry, Tokyo Gakugei University, Koganei, Tokyo 184-8501*

Supported molybdena are typical catalysts for olefin metathesis. It is accepted widely that reduced Mo ions such as Mo^{4+} and/or Mo^{5+} should exist as catalytically active center for metathesis. Thus, reductive pretreatment (with H_2 or CO) needs generally to reduce Mo^{6+} ions to form reduced ions as catalytically active species. However, we reported recently that molybdena supported on amorphous silica-alumina exhibit high activity for propene metathesis, which is a typical metathesis reaction, even at room temperature without reductive pretreatment.[1] In this study, it is concluded that support effect of silica-alumina strongly relate to not only structural change but also red-ox performance in contact with propene, and molybdena species on silica-alumina can easily be reduced to form reduced ions as metathesis active species in contact with propene. To obtain detailed structural information about the active molybdena species for metathesis, Mo L_{III}-edge XANES was applied to characterize the active molybdena species. The XANES spectrum probes the orbitals of 4*d* character participating in the Mo-O bonds. The white lines of the spectrum are split, corresponding to the ligand field splitting of Mo 4*d* orbitals. Thus the XANES spectrum is very sensitive to reflect the local structure of Mo ions. In this report, MoO_3/SiO_2-Al_2O_3 catalysts before/after propene metathesis were characterized by means of Mo L_{III}-edge XANES, and structural effect with red-ox behavior was studied in contact with propene.

Supported molybdena catalyst samples were prepared by impregnation of each metal oxide support with an aqueous solution of ammonium heptamolybdate (AHM). The oxide supports used were SiO_2 (Aerosil), Al_2O_3 (Nacalai), and amorphous SiO_2-Al_2O_3 containing 28.6 wt% (JRC-SAH-1, denoted as SAH-1) and 13.8 wt% (JRC-SAL-2, denoted as SAL-2) Al_2O_3. The impregnating solution was stilled at room temperature and evaporated at 343 K for 6 hours, and then the paste was dried for overnight and calcined at 773 K for 6 hours. The Mo L-edge XANES spectra were collected on a facility of BL-7A station of soft X-ray beam line at UVSOR, IMS, with 750 MeV of ring energy. Each powdery sample was mounted on a carbon-tape, and then attached on a beryllium-copper dynode in the first-stage of electron multiplier placed into a vacuum chamber. After the chamber had been evacuated (< 3.0•10-7 Torr), the spectrum was recorded in a total electron yield (TEY) mode at room temperature, using the Ge(111) double-crystal monochromator (2*d* = 0.6532 nm). The photon energy was calibrated by using Mo metal sample at Mo L_{III}-edge (2520 eV).

The Mo L_{III}-edge XANES spectra of supported molybdena samples and reference compounds are shown in Fig. 2 and 3. The detailed interpretation of the spectra was described elsewhere.[2] For MoO_3/SiO_2 and MoO_3/Al_2O_3 samples (Fig. 2), tetrahedral Mo-O_4 species are dominant at low MoO_3 contents (2.5 wt% in MoO_3/SiO_2 and 2.5 - 7.5 wt% in MoO_3/Al_2O_3). With an increase in MoO_3 content, polyanion-like Mo-O_6 octahedra coexist with tetrahedra. For 15.0 wt% MoO_3/SiO_2, the octahedral species exist mainly. These results support the conclusion reported previously by several workers.[3] On the other hand, the XANES spectra of MoO_3/SAH-1 before/after the reaction are shown in Fig. 3. Before the reaction, these spectra indicate that tetrahedral and octahedral species coexist in the whole molybdena contents, and tetrahedral molybdena species exist even at the higher MoO_3 contents. Thus it is suggested that SAH-1 support brings about the formation of disordered molybdena species with tetrahedral local structure. In many cases such as MoO_3/SiO_2, highly dispersed molybdena species on the support consist of tetrahedral Mo-O_4 species. However, the results of UV-Vis spectroscopy showed that the

molybdena on SAH-1 do not consist of highly dispersed tetrahedra but contain polyanion-like species mainly. In fact, it is hardly accepted in 15.0 wt% MoO_3/SAH-1 that highly dispersed tetrahedra are dominant. It may suggest that unique molybdena species are stabilized on SAH-1, and poorly crystallized polymolybdate species with tetrahedra exist mainly. Formation of bulk MoO_3 phase and/or large polyanion clusters proceeds hardly on SiO_2-Al_2O_3 because of peculiar support-interaction.[4] After the reaction at 473 K, molybdena species in 2.5 wt% MoO_3/SAH-1 shows a little change. For 7.5 - 15.0 wt% MoO_3/SAH-1, structural change of tetrahedral species is scarcely brought about by the reaction. In these samples, the white line of higher energy becomes lower by the reaction at 473 K, indicating the decrease of tetrahedra. The XANES of 7.5 wt% MoO_3/SAH-1 shows the most definite change. For this sample, the white line at higher energy side shows less intense with an increase in reaction temperature. Thus it is concluded that tetrahedral species decreases in contact with propene, and reduced Mo ions are formed at the same time. In many molybdena systems reported by many workers, octahedral species can be reduced easier than tetrahedral one.[5] In addition, isolated Mo^{6+}-O_4 tetrahedral species can hardly be reduced thermally. [6] However, tetrahedral molybdenum species on SAH-1 tend to decrease in contact with propene. Thus it can be proposed that tetrahedral species formed on SAH-1 should not isolated ones. In addition, the difference of XANES edge energy is less seen between before and after contact with propene. From the result of ESR, reduction of Mo^{6+} ions proceeds by propene contact. If Mo^{5+} exists mainly after the reaction, the edge energy should be shifted to lower energy. From these results, it is concluded that unique polymolybdate species on SAH-1 are easily reduced in contact with propene, but reduced ions are formed partly and Mo^{6+} ions are still dominant. At the same time, tetrahedral species are consumed during the reaction.

In this study, it is concluded that MoO_3/SAH-1, as a noted metathesis catalyst, consists of poorly-ordered polymolybdate species before the reaction. After contact with propene even at room temperature (293 K), Mo ions are partly reduced to form metathesis active species when tetrahedral species decrease. This red-ox behavior should be brought about by the support effect of SAH-1. It is suggested that the metathesis active sites are not highly dispersed Mo ions in reduced state but exist in poorly crystallized polymolybdena species with reduced ions partly.

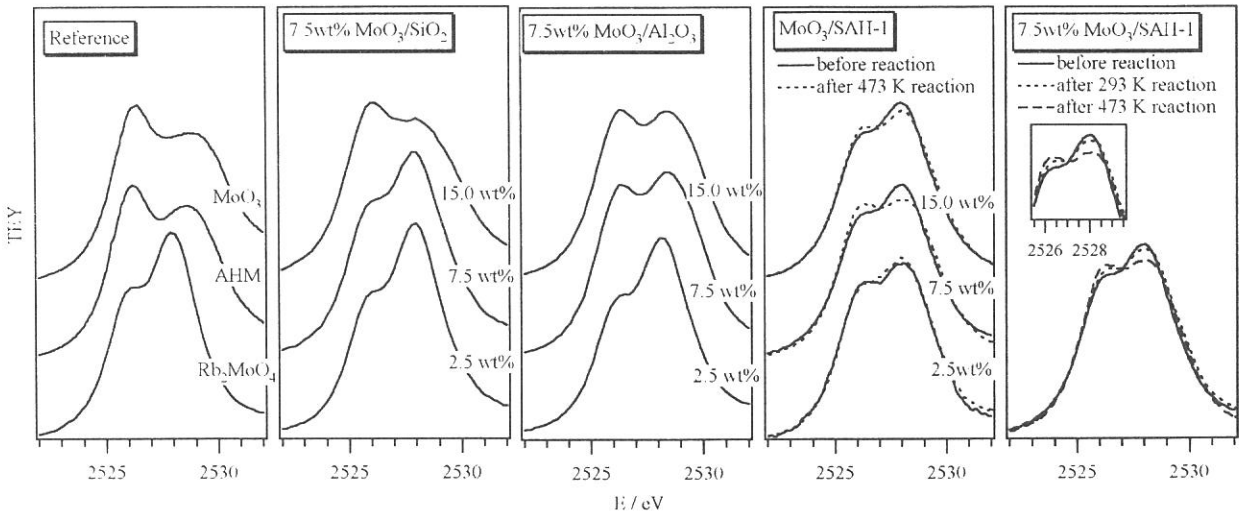

Fig. 1 Mo L_{III}-edge XANES spectra of supported molybdena samples and reference Mo compounds.

[1] H. Aritani, O. Fukuda, T. Yamamoto, T. Tanaka and S. Imamura, Chem. Lett., (2000) 66. [2] H. Aritani, T. Tanaka, T. Funabiki, S. Yoshida, K. Eda, N. Sotani, M. Kudo and S. Hasegawa, J. Phys. Chem., 100 (1996) 19495. [3] H. Shimada, N. Matsubayashi, T. Sato, Y. Yoshimura, A. Nishiyama, N. Kosugi and H. Kuroda, J. Catal., (1992) 746.; H. Prialiaud, Proc. 3rd Int. Conf. Chemistry and Uses of Molybdenum, eds. P. C. H. Mitchell and A. Seamans (Climax Molybdenum Co., Ann Arbor, Michigan, 1976), pp. 195. [4] S. Rajagopal, J. A. Marzari and R. Miranda, J. Catal., 151 (1995) 1995.; S. Rajagopal, H. J. Marini, J. A. Marzari and R. Miranda, J. Catal., 147 (1994) 417. [5] F. E. Massoth, Adv. Catal., (1978) 265.; A. Ueno, Y. Kotera, S. Okuda and C. O. Bennett, Proc. 4th Int. Conf. Chemistry and Uses of Molybdenum, eds. P. C. H. Mitchell and A. Seamans (Climax Molybdenum Co., London, 1982), pp. 250. [6] C. Louis and M. Che, J. Phys. Chem., 91 (1987) 2875.; B. N. Shelimov, I. V. Elev and V. B. Kazansky, J. Catal., 98 (1986) 70.

(BL7A)

Mg-K edge absorption study of MgO-ZnO solid solutions

Teruyasu MIZOGUCHI,[A] Kazuyoshi TATSUMI,[A] Masanobu NAKANO,[A]
Fumiyasu OBA,[A] Masato YOSHIYA,[A] Hirohiko ADACHI,[A] Isao TANAKA,[B]
Tomoko YOSHIDA[C], Hisao YOSHIDA,[D]
Shang-Di MO[E] and Wai-Yim CHING[E]

[A] *Department of Materials Science and Engineering, Kyoto University, Sakyo, Kyoto 606-8501 Japan*
[B] *Department of Energy Science and Technology, Kyoto University, Sakyo, Kyoto 606-8501 Japan*
[C] *Center for Integrated Research in Science and Eng., Nagoya University, Nagoya, 464-8603, Japan*
[D] *Department of Applied Chemistry, Nagoya University, Nagoya, 464-8603, Japan*
[E] *Department of Physics, University of Missouri-Kansas City, Kansas City, Missouri 64110-2499, USA*

Solid solutions of ceramic materials are widely used in modern technology. However, their atomic/electronic structures have not been clarified in most of the cases. X-ray absorption is a versatile tool having potential to elucidate the local atomic/electronic structures of selected atoms. However, it has not been widely applied in ceramic science. One of the greatest reasons is due to the lack of good theoretical tools to interpret experimental spectra. Experimental spectra have thus far been compared with some spectra from reference materials. Information obtained by such a "finger-printing" method is naturally very limited. We have to make a combined effort between experimental XANES and theoretical analysis of the spectra.

High purity MgO powder (2000A, Ube Materials Industries, Japan) and ZnO powder (Seido Chemical Corp., Japan) were used as starting materials. Two powders were mixed by magnetic-starrier for 3h in ethanol. Sintering was done in air at 1623K for 3h for undoped ZnO, and 1933K for 3h for the doped/undoped MgO. The Zn-doped MgO shows only a single crystalline phase of a rock-salt structure by a standard powder x-ray diffraction method. The XAFS were obtained at BL-7A of UVSOR/IMS. Mg-K edge spectra were collected in a total electron yield mode at room temperature using a beryl two-crystal monochrometer. Samples were put on the first photocathode of electron multiplier using adhesive carbon tape.

Figure 1 shows Mg-K edge XANES from four samples with different ZnO concentrations. The series of the spectra shows a continuous change. Relative intensity of the first peak decreases with the increase in Zn-concentration. At the same time, the peak located at around 1310 eV show notable shift toward low energy with rising the Zn-concentration. In the companion paper in this issue, we reported the Zn-$L_{2,3}$ edge XANES from the solid solutions. They are clearly different from the Zn-$L_{2,3}$ edge XANES of wurzite ZnO having 4-fold coordinated Zn. The results confirmed the presence of 6-fold coordinated Zn in the solid solutions. The Mg-K edge XANES should therefore be interpreted by taking the fact into account. Figure 2 shows theoretical XANES by a first principles supercell calculation using the OLCAO (orthogonalized linear combination of atomic orbitals) method. As can be found, the theoretical spectrum can reproduce the experimental XANES quantitatively when a sufficiently large super-cell is used to take into account core-hole effects correctly. Details of the computational procedure can be found elsewhere

[1]. When theory has sufficient predictive power as in the present study, the combined work with good experimental tools should really be useful for elucidating the local atomic/electronic structures of solute atoms. Near edge structures of the core-loss spectra of the electron energy loss spectroscopy (ELNES) is another important tool to provide similar information to XANES. Since ELNES can be measured using a modern transmission electron microscope, it is sometimes more easy to measure than the XANES. In the case of Mg-K edge study, however, the energy resolution as well as the S/N ratio is far better in the XANES as can be seen in Fig. 2.

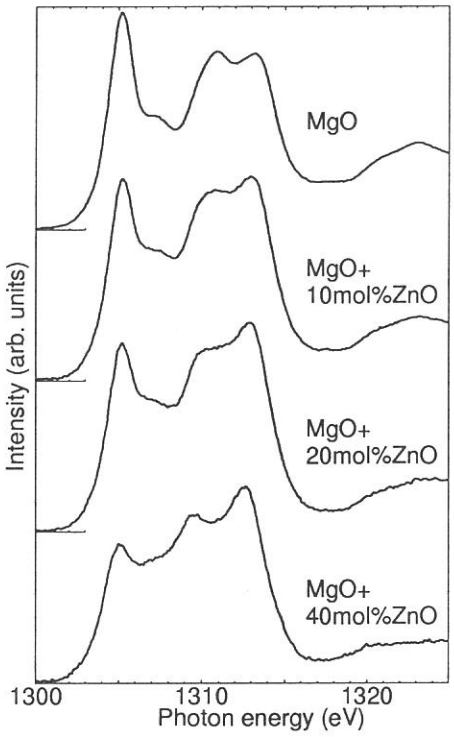

Fig.1 Experimental Mg-K edge XANES from pure MgO and MgO-ZnO solid solutions.

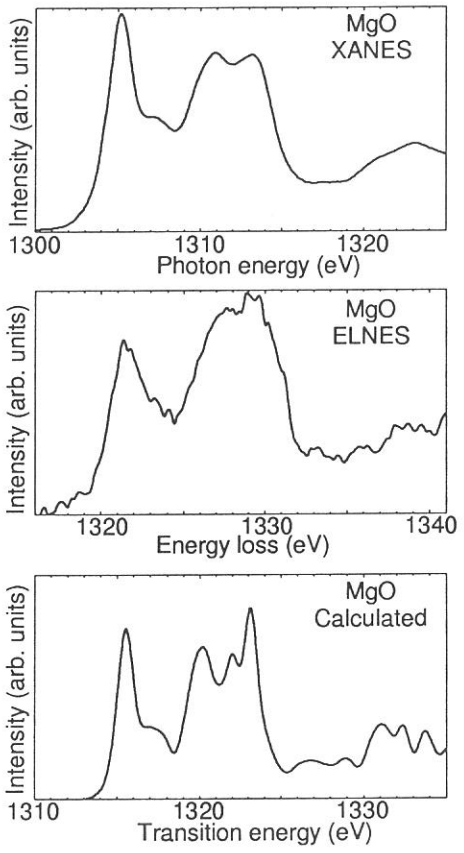

Fig.2 Experimental Mg-K edge XANES and ELNES from pure MgO. Theoretical XANES by the OLCAO calculation using 128 atoms-supercell is shown for comparison.

Acknowledgements This work was supported by Grant-in-Aid for Scientific Research on Priority Areas (No. 751) from Ministry of Education Science, Sports and Culture of Japan .

REFERENCES

[1] Shang-Di Mo, W. Y. Ching, Phys. Rev. B **62** (2000) 7901.

(BL7A)

Zn-$L_{2,3}$ edge absorption study on six-fold coordinated Zn in MgO

Isao TANAKA,[A] Teruyasu MIZOGUCHI,[B] Kazuyoshi TATSUMI,[B] Masanobu NAKANO,[B]
Fumiyasu OBA,[B] Masato YOSHIYA,[B] Hirohiko ADACHI,[B]
Tomoko YOSHIDA[C], Hisao YOSHIDA,[D]

[A] *Department of Energy Science and Technology, Kyoto University, Sakyo, Kyoto 606-8501 Japan*
[B] *Department of Materials Science and Engineering, Kyoto University, Sakyo, Kyoto 606-8501 Japan*
[C] *Center for Integrated Research in Science and Eng., Nagoya University, Nagoya, 464-8603, Japan*
[D] *Department of Applied Chemistry, Nagoya University, Nagoya, 464-8603, Japan*

Small amount of dopants often changes properties of ceramic materials dramatically. However, their atomic/electronic roles have not been clarified in most of the cases. The lack of such information often limits further development of ceramic materials. In the present study, we investigate local structures around Zn^{2+} solute in MgO, which can be a good model system to demonstrate the usefulness of the x-ray absorption method to study the local structures of impurities in ceramic materials.

MgO possesses a simple rock-salt structure. The lattice relaxation associated with the substitution is expected to be simple. Solubility limit of Zn^{2+} in MgO was reported to be 38.7mol% at 1873K [1]. Zn^{2+} is therefore expected to occupy the six-fold coordination site in MgO. Very recent XAFS data confirmed the six-fold coordination [2]. Zn^{2+} in wurzite-ZnO (w-ZnO) or related oxides usually exhibits 4-fold coordination except for the case of high-pressure ZnO having a rock-salt structure (c-ZnO) [3]. We compare Zn-$L_{2,3}$ edge ELNES from w-ZnO and Zn^{2+} doped MgO to see the difference in spectral features between the 4-fold and 6-fold coordinated Zn atoms. Special interests are placed on the analogy to the difference between the Si-$L_{2,3}$ edge ELNES from 4-fold and 6-fold coordinated Si, i.e., α-quartz and stishovite.

In a companion paper, we report Mg-K absorption study of the MgO-ZnO solid solutions. Experimental procedure has been described there. The XAFS were obtained at BL-7A of UVSOR/IMS. Zn-$L_{2,3}$ edge spectra were collected in a total electron yield mode at room temperature using a beryl two-crystal monochrometer.

Figure 1 (left) companion paper included in this issue experimental Zn-$L_{2,3}$ edge XANES from w-ZnO and 10mol%ZnO-doped MgO. The w-ZnO shows four major peaks, while Zn^{2+} in MgO displays only three in the energy range shown in the figure. The major difference can be simply ascribed to the difference in the coordination numbers, i.e., four in w-ZnO and six in Zn-doped MgO.

Si^{4+} in SiO_2 exhibits 4-fold coordination in α-quartz and 6-fold coordination in stishovite. Their Si-$L_{2,3}$ edge XANES have been reported by some groups [4, 5, 6], which agree well with each other. Figure 1 (right) shows the results by Li et al [4]. The 4-fold coordinated Si basically exhibit four sets of peaks in the energy region, whereas the 6-fold coordinated Si shows three-sets. Although the $L_{2,3}$ edge spectra from Zn and Si do not resemble each other at first sight, the origin of the sets is identical: It is derived from the point symmetry within the first coordination unit. Figure 2 schematically shows how the peaks are made out of the molecular orbitals of the primitive units. For simplicity, $(ZnO_4)^{6-}$ and $(ZnO_6)^{10-}$ are taken to be in

tetrahedral (T_d) and octahedral (O_h) symmetries.

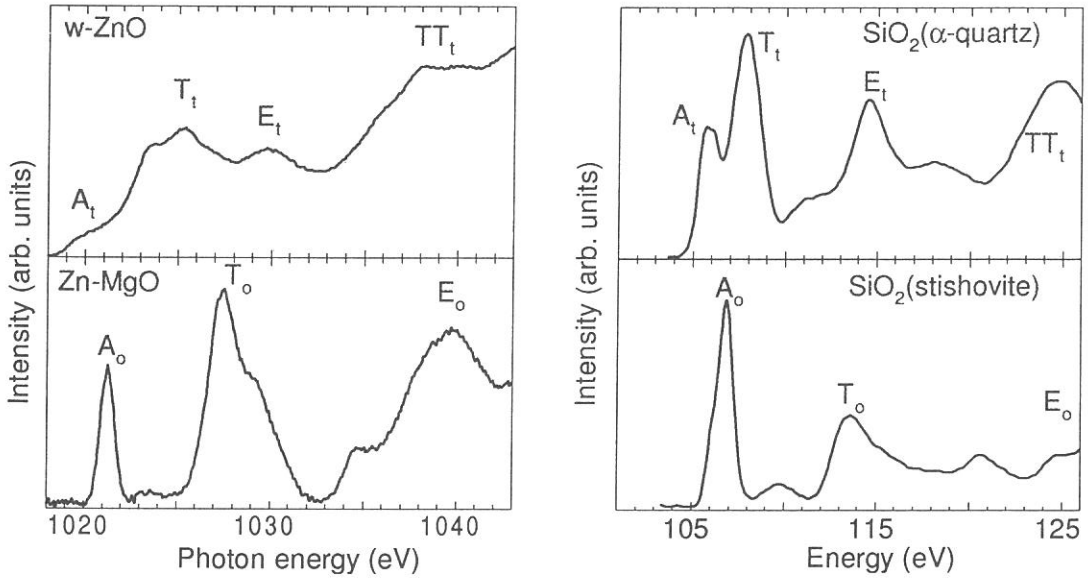

Fig.1 (Left) Experimental Zn-$L_{2,3}$ edge XANES from w-ZnO and 10mol% ZnO doped MgO obtained in the present study. (Right) Experimental Si-$L_{2,3}$ edge XANES for α-quartz and stishovite-type SiO_2 as reproduced from Ref. 4.

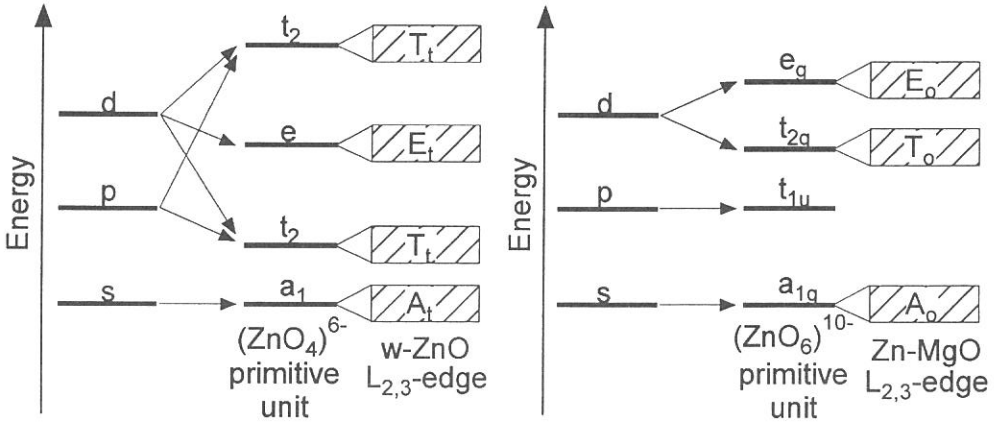

Fig.2 Mechanism of the formation of spectral features of the Zn-$L_{2,3}$ edge XANES from the molecular orbitals of the corresponding primitive units.

Acknowledgements This work was supported by Grant-in-Aid for Scientific Research on Priority Areas (No. 751) from Ministry of Education Science, Sports and Culture of Japan .

REFERENCES

[1] E. R. Segnit, S. E. Hlland, J. Am. Ceram. Soc., **8** (1965) 409.
[2] T. I. Nedoseikina, A. T. Shuvaev, V. G. Vlasenko, J. Phys.: Condens. Matter **12** (2000) 2877.
[3] C. H. Bates, W. B. White, R. Roy, Science **137** (1962) 993.
[4] D. Li, G. M. Bancroft, M. Kasrai, M. E. Fleet, X. H. Feng, K. H. Tan, B. X. Yang, Solid State Commun. **87** (1993) 613.
[5] T. Sharp, Z. Wu, F. Seifert, B. Poe, M. Doerr, E. Paris, Phys. Chem. Minerals **23** (1996) 17.
[6] D. J. Wallis, Ph. D. Thesis, University of Cambridge, 1994.

(BL-7A)

Al *K*-XANES spectra of AlN/Fe multilayered thin films

Masao Takahashi, Akira Asano, Yoshiko Kasama and Hikaru Kobayashi

ISIR, Osaka University, 8-1 Mihogaoka, Ibaraki, Osaka 567-0047

Introduction

Several species are known in the Fe-N system, i.e., α″-$Fe_{16}N_2$, γ′-Fe_4N, ε-$Fe_{2-3}N$, ζ-Fe_2N and γ″ and γ‴-FeN_y. Among them, iron nitrides with the low nitrogen content have become of an intensive interest after it has been reported that α″-$Fe_{16}N_2$ takes saturation magnetization larger than that of α-Fe.[1] By a reactive sputtering deposition, on the other hand, two iron nitrides, γ″ and γ‴-FeN_y which have not been reported on the equilibrium phase diagram have been prepared and γ‴-FeN_y with Rock salt-like crystal structure takes iron having larger magnetic momentum than α-Fe.[2] Iron nitrides, having both high hardness and corrosion resistance in addition to their magnetic property, therefore, have attracted much attention for one of promising magnetic materials. However, such iron nitrides with fascinating magnetic property are almost thermally unstable. A formation of composites or layered films with non-magnetic and thermally stable material has recently been investigated for an application of such nitrides to a practical magnetic material. It has been reported for multilayered Fe/AlN films that the value of the saturation magnetization of iron could be controlled by regulating thickness of each layer.[3] Fe *K*-XANES spectral feature of these multilayered films was getting different with increasing number of layers in the film, ie., with an increment of the number of the interface, suggesting that the nitridation of iron has occurred at the interface between AlN and Fe films. Al *K*-XAFS spectra for such multilayered Fe/AlN films and AlN film deposited on Fe thick film could elucidate the coordination state of Al near the interface. In the present study, Al *K*-XANES spectra for those films have been compared with that of AlN film.

Experimental

Films were prepared using two target-type rf-sputter deposition apparatus(JEH-430RS, JEOL). Al and Fe metal targets were used for deposition of AlN and Fe, respectively. AlN film was deposited under nitrogen atmosphere, while argon gas was used for formation of Fe film. A silica grass slide was used as a substrate. A base pressure of the deposition chamber was below 1×10^{-4} Pa and the deposition chamber was evacuated down to the base pressure before the deposition of each layer. The sputter gas pressure was kept at 1 Pa and the rf power of 30 or 100 W was applied. Film thickness was controlled by the deposition duration and total film thickness of the multilayered film was 1 μm. $[AlN/Fe]_n$ denotes a multilayered film having *n* layer(s) of both AlN and Fe. Films were preserved in *n*-hexane.

Al *K*-XANES spectra were measured at BL-7A. YB_{66} was used for the monochromator crystal. Graphite powders were very thinly spread on top of the surface of sample film. The sample film was stuck on the inner surface of first dinode of the electron multipler with a conductive adhesive tape. The total electron yield method was used for the measurement. Gold mesh transmitting 80% of photons was used for the monitor of I_0 current.

Results and Discussion

Al *K*-EXAFS spectra measurements have been executed at BL-7A but unfortunately spectra with good S/N ratio have not been obtained due to the insufficient photn flux, because the wiggler had not been working well.

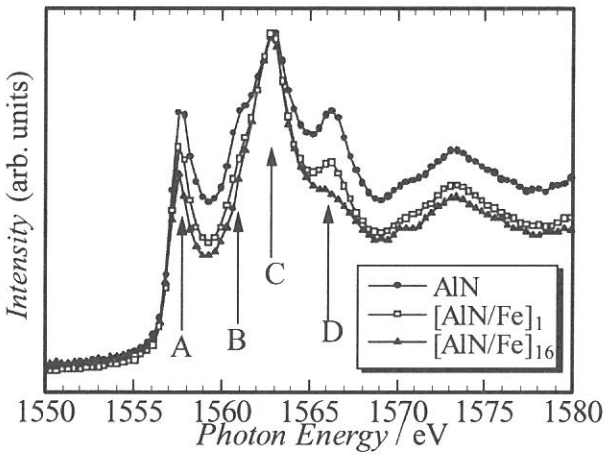

Fig. 1. Al K-XANES spectra for the AlN film and multilayered films, $[Al/FeN]_n$. Full circles, open squares and solid triangles show AlN, $[Al/FeN]_n$ with n = 1 and 16, respectively.

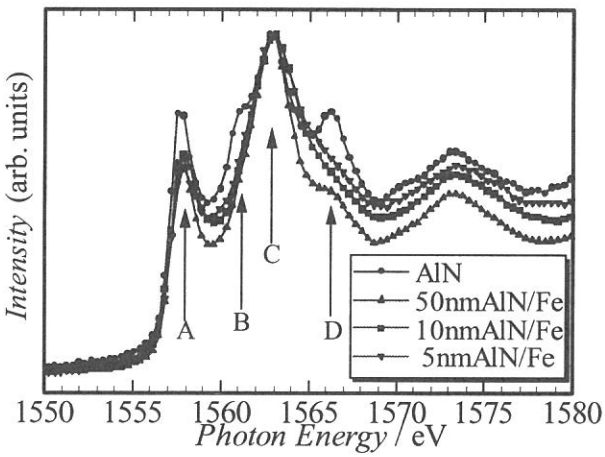

Fig. 2. Al K-XANES spectra for AlN and AlN/Fe films. Circles, triangles, squares and lozenges denote the AlN film and AlN/Fe films with AlN thickness of 50, 10 and 5 nm, respectively.

Instead, Al *K*-XANES spectra have been measured. Though the electronic structure is obtainable from the XANES, the EXAFS, which prolongs more than 1500 eV above the absorption edge, is valuable for the local structure determination. Therefore, the beam line where one can measure the EXFAS with good S/N ratio is required.

Al *K*-XANES spectra for $[AlN/Fe]_n$ multilayered films and AlN/Fe films are shown in Figs. 1 and 2, respectively. There are four peaks, A - D, between photon energy of 1555 and 1570 eV. All spectra in Figs. 1 and 2 are normalized as the peak C of all spectra coincides each other. The intensity of peaks A, B and D apparently decreases with an increase of number of layers, n in $[AlN/Fe]_n$, (Fig. 1) and with a decrease of the film thickness (Fig. 2). The increase in n means the increase of the interface between AlN and Fe layers and the decrease of thickness of AlN layer. The spectrum is measured as the convolution of signals from both the bulk and the interface. The thinner the AlN layer is , the more the spectrum includes information around the interface. Therefore, the change in the spectral shape appears to indicate that the electronic structure of Al at the AlN/Fe interface differs from that of the bulk AlN.

It may be considered from the present change in the spectral shape that a certain kind of thin film effect causes such spectrum change, that is, the electronic structure of AlN itself alters as thickness of the AlN layer decreases. The XPS depth-profile measurements have been showed the possibility of the elimination of nitrogen atoms from AlN at the AlN/Fe interface. Moreover, both the Fe *K*-XANES study and the magnetic property of multilayered $[AlN/Fe]_n$ films point out the posibility of existence of iron nitride, FeN_y. These evidences have supported the existence of the different species from AlN in the vicinity of the interface. Theoretical considerations on the Al *K*-XANES spectra are required to deduce the coordination structure around Al atoms and are presently progressed.

References

1) T.K.Kim and M.Takahashi, *Appl. Phys. Lett.*, **20** (1972) 492.

2) M.Takahashi, H.Fujii, H.Nakagawa, S.Nasu and F.Kanamaru, *Proc. 6th Int Conf. Ferrites*, **1992**, 508.

3) S.Kikkawa, M.Fujiki, M.Takahashi and F.Kanamaru, *Ceramic Microstruct.: Control at the Atomic Level*, ed. by A.P.Tomsia and A.Glaeser, Plenum Press, N.Y., 1998, pp. 605.

(BL7A)

The measurement of soft X-ray excited optical luminescence of a silica glass

Tomoko Yoshida[1], Tetsuo Tanabe[1] and Tatsuya Ii[2]

[1]*Center for Integrated Research in Science and Engineering, Nagoya University, Nagoya 464-8603, Japan*

[2]*Department of Nuclear Engineering, Graduate School of Engineering, Nagoya University, Nagoya 464-8603, Japan*

Introduction

The radiation effects on silica glasses are one of the main concerns for their application as optical windows, insulators and optical fibers under the severe environments such as fusion and fission reactors.[1] Recently, we have made in-situ luminescence measurements of silica glasses induced by in-reactor irradiation, and the in-reactor luminescence was found to be a powerful technique to observe dynamic effects on the electrical property of a silica.[2] However, the detailed effects are still unknown, mainly because many kinds of radiations over the range from γ-ray to optical lights generate and interact each other with a silica in the reactor, which sometimes confused our understanding of dynamic radiation effects. In the present study, to take notice of the effects of soft X-ray, we tried to measure the luminescence from silica glasses under the irradiation of soft X-ray near Si K-edge.

Experimental

The samples used in this work were fused silica glass (T-2030) and synthesized silica glass (T-4040) of 13 mm diameter and 2 mm thickness produced by Toshiba Ceramics, Japan, with different OH content. Nominal impurity levels in these samples are listed in Table 1. The measurement of luminescence of the silica glass induced by soft X-ray irradiation (1.8-1.9 keV) were carried out on the beam line 7A at UVSOR, Insitute for Molecular Science with a stored current of 100-200 mA. The luminescence was focused by a lens in the UVH chamber to the monochromator (CP-200, SEIKO EG&G) and detected by a multi-channel analyser (OMA III, SEIKO EG&G). The photon detecting efficiency especially above 4 eV was reduced.

Results and Discussion

Fig. 1 shows the photoluminescence spectra of a fused silica glass (T-2030) obtained under excitation at various energy (5.1-7.7 eV). These spectra were recorded at BL1B at UVSOR. Two prominent PL bands at 3.1 eV and 4.2 eV were observed. Thomon *et al.*[3] reported the existence of two B_2 bands excited at 5.1 eV, and it is commonly accepted that the PL emission bands at 2.7 eV and 4.4 eV are attributed to the $B_{2\alpha}$ while the $B_{2\beta}$ center generates the 3.1 eV and 4.2 eV PL bands. Therefore, the PL bands for the low-OH fused silica glass (T-2030) are very likely originate from a fair amount of intrinsic oxygen deficiencies assigned as B2β exist in this silica glass.

On the other hand, we succeeded luminescence measurement of the same silica glass under the irradiation of soft X-ray near Si K-edge (ca. 1.83 keV) as shown in Fig. 2, although the energy resolution of this spectrum was very low at the present stage. One can see the similar emission band around at 3.2 eV, therefore, it is very likely that this luminescence mainly originates from

Table 1

Nominal impurity levels in silica glasses (in ppm)

Sample	Al	Fe	Na	K	Cu	B	OH
Fused silica (T-2030)	8	0.8	1	1	0.02	0.3	1
Synthesized silica (T-4040)	0.1	0.05	0.05	0.05	<0.01	<0.01	800

the oxygen deficiencies in the silica glass due to an electron excitation during soft X-ray irradiation. We tried to measure the luminescence of a synthesized silica glass (T-4040) which has few intrinsic defects, and confirmed that no prominent emission band was observed.

In our next study, it will be an important subject to investigate the change in the intensity of the luminescence with the soft X-ray energy as well as its irradiation time.

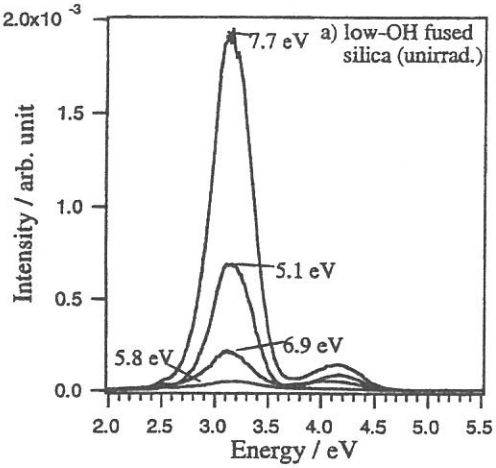

Fig. 1 The photoluminescence emission spectra excited at various energies in a low-OH fused silica glass (T-2030).

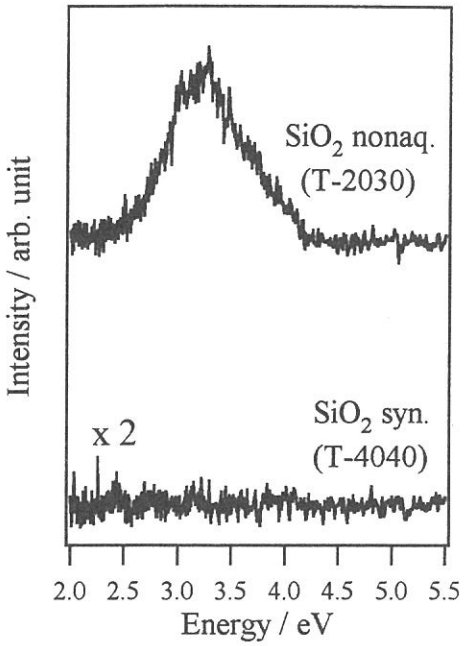

Fig. 2 X-ray excited optical luminescence spectra of silica glasses.

Acknowledgments

The authors are grateful to Prof. Eiji Sigemasa, Prof. Masao Kamata and Mr. Eiken Nakamura of UVSOR for their great help and cooperation in the luminescence measurements.

References

[1] F. W. Clinard Jr., L. W. Hobbs, in : Physics of Radiation Effects in Crystal, Elsevier, Amsterdam, 1986, p. 442.

[2] M. Fujiwara, T. Tanabe, H. Miyamaru and M. Miyazaki, Nucl. Inst. And Meth. B 116 (1996) 536.

[3] R. Tohmon, H. Mizuna, Y. Ohki, K. Sasagane, K. Nagasawa, and Y. Hama, Phys. Rev. B 44 (1989) 1337.

(BL7A)

Improvement electrochemical properties of surface treated natural graphite by aluminum and its mechanisms from Al K-edge XANES

Sung-Soo Kim, Yoshihiro Kadoma, Hiromasa Ikuta, Yoshiharu Uchimoto, and Masataka Wakihara
Department of Applied Chemistry, Graduate School of Science and Engineering, Tokyo Institute of Technology
Ookayama, Meguro, Tokyo 152-8552, Japan.

The rechargeable lithium ion batteries, using a carbon material as anode and transition metal oxide such as $LiCoO_2$, $LiMn_2O_4$ or $LiNiO_2$ as cathode, have been developed. During the past years, there have been a lot of research works to improve of the battery performance carried out on various kinds of carbonaceous material ranges from graphite to disordered carbon by control of various properties such as structure, surface modification[1-3]. Among the several types of carbonaceous materials, natural or synthetic graphitic carbons are commonly found in most commercial products in the market today due to their merits such as flat and low working voltage with respect to lithium metal, relatively high coulombic efficiency, etc. Specifically, natural graphite can be thought as potential materials for anode in lithium ion battery in terms of cost[4]. However, it has been difficult to control the key parameters of natural graphite that affect their characteristics for use as anode because carbon materials have large variations in their electrical properties. Especially, surface properties of natural graphite frequently affect the electrochemical performances such as reversible specific capacity, cycle life, rate capability. Therefore it has been desired to improve by control surface properties of natural graphite. In this work, we investigated the influence of surface and/or structure modification of natural graphite by introducing aluminum compound for electrochemical performances of anode in lithium ion battery. The local structure of amorphous-like alumina on surface of natural graphite was investigated by Al K-edge XANES.

The Aluminum-treated samples were prepared by aluminum tri-etoxide($Al(OC_2H_5)_3$, Soekawa Chemicals) treatment on NG2(Kansai chemicals). The NG2 graphite was soaked in ethanol solution containing 10wt% aluminum tri-etoxide, followed by ultrasonic treatment for 3 hours, filtration and drying above 200°C for 1 day to remove residual of ethanol. The electrochemical measurement was carried out with the use of CR2032 coin-type cell. The working electrodes were prepared by doctor-blade technique on copper foil, spreading paste consisted of 10wt% polyvinylidenefluoride(PVdF) as binder, 10wt% acethylene black as conductive agent, 80wt% treated or pristine NG2 graphite and appropriate amount of 1-methyl-2-pyrrolidinone(NMP) as solvent. After drying of NMP solvent, the electrode was cut into disk(the weight of all sample was controlled around 4mg). Lithium metal was used as counter electrode. The electrolyte used was 1M $LiClO_4$ dissolved in ethylene carbonate(EC)/diethylene carbonate(DEC)(volume ratio 1:1). The cell assembly was operated in a glove box filled with argon gas. The specific capacity was measured by galvanostatically with current density 350mA/g in the ranges between 0 and 2.5V. Al K-edge XAS were measured on BL7A at UVSOR with a ring energy of 750MeV and a stored current of 70-220mA in a mode of total electron yields. The KTP double crystal monochromator was used. The monochromator scanning angle step width was 0.003°, which corresponds to *ca.* 0.1eV at 1560eV.

FT-IR spectra of untreated and Al-treated NG2 samples which were dried at various tempera-

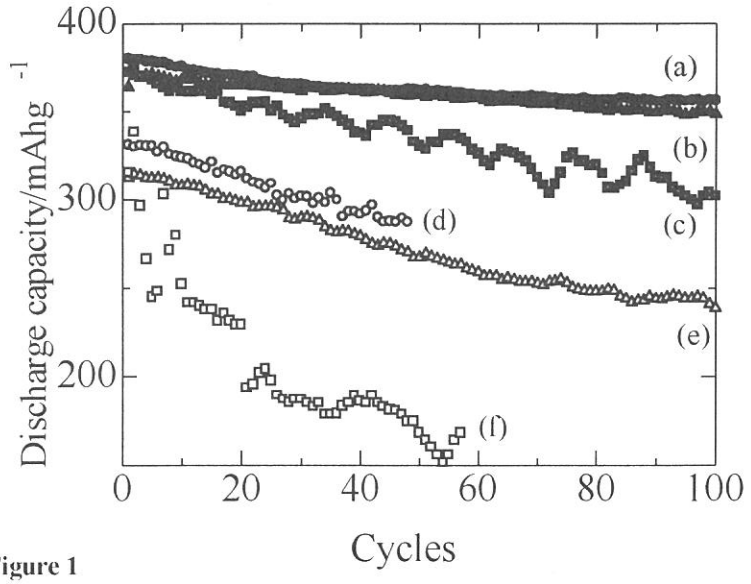

Figure 1
Cycle performances with C-rate of pristine and Al-treated sample. The circle, triangle and rectangular plot respresent 0.2C, 0.5C and 1.0C-rate, respectively. The simple plot and boldic one shows untreated and treated samples, respectively. : (a)treated 0.2C, (b)treated 0.5C, (c)treated1.0C, (d)untreated 0.2C, (e)untreated 0.5C and (f)untreated 1.0C.

ture together with aluminum tri-etoxide ethanol solution. In Spectra of $Al(OC_2H_5)_3$ ethanol solution and Al-treated at 120°C. the band around 1100 cm^{-1} can be attributed to the C-O stretching vibration of ethoxy groups was observed. On the other hand. the band disappeared in dried sample at 200°C and untreated graphite. This result indicates that residual of ethoxy groups at 120°C and the complete removal of ethoxy groups and ethanol solvent takes place above 200°C.

X-ray measurements of untreated and Al-treated NG2 indicated almost consistency in their XRD patterns with no changes in d(002) values. Eventually. we couldn't detect the remarkable influence of small amounts of Al on surface by XRD. which is measurement of total bulk structure. There was noticeable change between untreated and treated graphite in Raman spectroscopy. which reveals mainly the surface structure to the extent of several tens of nanometer. It is well known that graphite shows an intense band at 1580cm^{-1} indicates an E_{2g} vibration mode in the graphite region of carbon(G-band) and relatively weak one at 1360cm^{-1} is an A_{1g} mode arising from the disordering in carbon(D-band) which is Raman inactive for perfect graphite crystals. We could observe the frequency shift and intensified G-band with Al-treatment which is similar phenomena due to the formation of dilute stage1 in initial lithium intercalation. whereas no remarkable changes in D-band. Accordingly the relative intensity $R(I_D/I_G)$. which indicates the ratio of graphite edge plane to the graphite plane. decreased with Al-treatment of surface. The small peak around 1560cm^{-1} due to the oxygen and 1290cm^{-1} in untreated sample is disappeared in Al-treated graphite. Though we could not observe bulk structure change in XRD measurement. the results of Raman spectroscopy is enough to suggest that the Al-treatment causes remarkable modification on graphite surface.

In Fig. 1. the cycle life performance of untreated and Al-treated graphite electrode was represented. The Al-treated graphite shows clearly improved cycle performance compared to untreated one. The periodic fluctuation of capacity in 1C rate (350mA/g) samples can be ascribed to the temperature variation of the testing atmosphere.

To investigate the structure of alumina on the surface of graphite. we measured the Al-K edge XANES. Since accurate structure of alumina are not known except θ -Al_2O_3. the structural analysis of amorphous-like alumina is not so simple. Recently. Al-K-edge XANES measurement combining quantitative analysis was proposed to estimate the local structure of alumina[5]. Only AlO_4 tetrahedra in mordenite was observed. whereas θ - Al_2O_3 has equally distributed between tetrahedral and octahedral coordinations of Al-atoms. It is known that the XANES spectra of AlO_4 tetrahedra and AlO_6 octahedra were clearly identified. A white line 1566eV is characteristics of AlO_4 compound and the peaks at 1568eV and 1572eV can be assigned to AlO_6 octahedral compound. In Fig.3, normalized XANES spectra with calcination temperature of Al-treated graphite samples were shown. We can observe a peak at 1565eV due to AlO_4 and two peaks at 1567eV and 1570eV due to AlO6 and the difference of peak position of AlO_4 and AlO_6 was about 2eV. In addition, the relative intensity of AlO_4 and AlO_6 was varied by calcination temperature. In the range of this study up to the 500°C of calcination temperature. the portion of AlO_4 increased. according to previous report[5], this alumina phase can be thought as boehmite+ γ type alumina. Comparing with the results of rate capability improvement of Al-treated samples (Fig.2). we can assume tetrahedral coordination of Al is more favorable in surface of graphite.

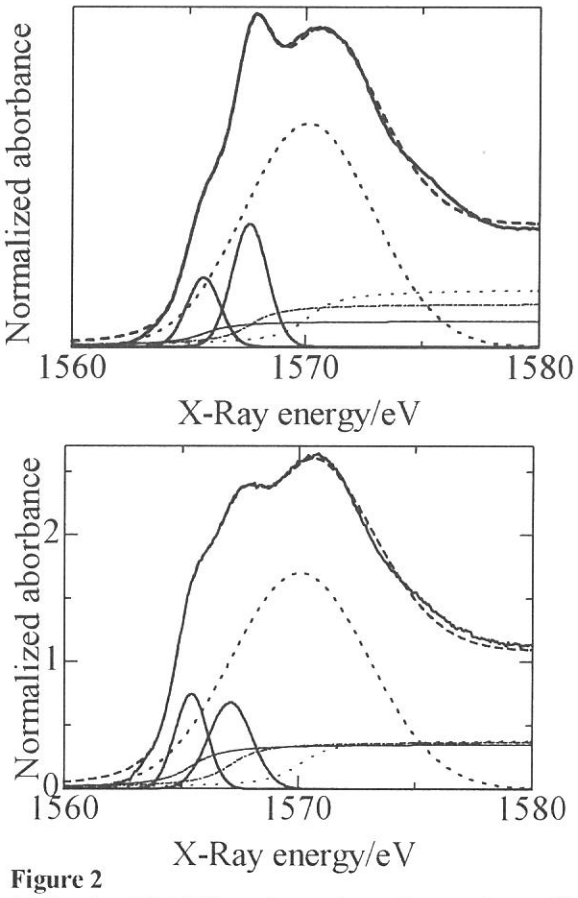

Figure 2
Al K-edge XANES on the surface of natural graphite and its simulated spectrum which composed of three sets of Gaussian and arctangent function. Each samples were calcined at (a) 300°C. and (b) 500°C.

Refedences

[1] E. Peled. G. Menachem. D. Bar-Tow. A. Melman. *J. Electrochem. Soc.*, **143**. L4 (1996).

[2] T. Nakajima. M. Koh. R.N. Singh. M. Shimada. *Electrochim. Acta*. **44**. 2879 (1999).

[3] K.Sumiya. J.Suzuki. R.Takasu. K.Sekine. T.Takamura. *J.Electroanal.Chem.*,**462**. 150 (1999).

[4] K. Fukuta. K. Kikuya. K. Isono. M. Yoshio. *J. Power Sources*, **69**. 165 (1997).

[5] K.Shimizu. Y.Kato. T.Yoshida. H.Yoshida. A.Satsuma and T.Hattori. *Chem. Commun.*,**1999**. 1681 (1999).

(BL7A)

Rb-L Absorption Spectra and Excitation Spectra of Photoluminescence of RbBr

Masahiro MORI, Takashi IKEDA, Takaaki AWATA[‡] and Tokuo MATSUKAWA[‡]

School of Informatics and Sciences, Nagoya University, Nagoya 464-8601
[‡] *Naruto University of Education, Naruto, Tokushima 772-8502*

(5: Solid- & liquid-phase spectroscopy 2; soft x-ray, absorption, photo-luminescence)

Soft x-ray excitation spectra of photoluminescence were measured in Rb- and Br-L region as well as the absorption spectra of RbBr. Both the photon energies of Rb- and Br-L edge exist near 1800eV, where only few spectroscopic studies are reported. One of the reasons is that a proper monochromator crystal has been poor, being able to utilized in the soft x-ray region. At the BL7A beam line, stable spectroscopic works have become recently possible by the use of KTP crystal in the photon energy region. The beam line is composed with a double crystal monochromator. We have already performed Br-L absorption measurements on some kinds of alkali bromides.

The purpose is to observe soft x-ray absorption spectra of both Rb- and Br-L edges on RbBr and discuss the excitation spectra of the visible (or/and ultraviolet) light obtained simultaneously. The samples – RbBr thin powder samples – were prepared with the vacuum evaporation on the polyester 2μm thin film and transferred to the sample preparation chamber for each measurement on every sample with different thickness. All measurements were carried out at room temperature. The absorption spectra were obtained by the total photoelectron yield. The excitation spectra were obtained simultaneously with recording the intensity of the visible (ultraviolet) light from the sample. A photo-multiplier tube for the photoluminescence was installed at 45 degrees to incident light direction through a quartz focusing lens of 20mm diameter at 200mm from the sample position. The absorption spectra were obtained by the total photoelectron yield. An electron-multiplier with a Be-Cu anode was set behind the sample film.

Figures 1 and 2 show comparisons of the absorption and the excitation spectrum of RbBr with two kinds of thickness; s. A is 45nm in thickness and s. B is 199nm in thickness. The absorption spectra have a series of fine structures at the edge commonly. Both absorption intensity distribution spectra are the similar with each other, and these have two absorption components which the one on the lower energy results from Rb-L_2 absorption edge and the other on the higher is originated from Rb-L_3 absorption. The Rb-L spectra show no overlap structures because of the large separation of around 50eV between L_2 and L_3 levels. The excitation spectra appear to follow the features of the absorption spectra except the absolute

val"e of the absorption edge depth. In the higher energy region luminescence yields show some structures which corresponds absorption structures as peaks to dips. Thus the excitation spectrum of RbBr shows inverted profiles of the absorption spectrum. It is a well known phenomenon in the ease the luminescence excitation spectra excited with x-ray. Emura *et al.* discussed that the excitation spectra change the profiles among the effective thickness of samples according to a phenomenological model. Their results show that the excitation spectra change their spectral features as the effective thickness change and finally reach the inverted profiles of absorption spectra.

Fig.1

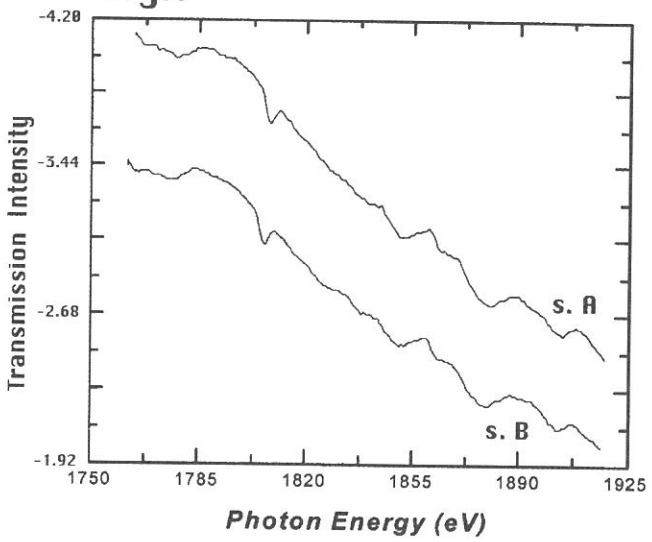

Figure 3 shows the excitation spectrum of RbBr single crystal whose thickness is sufficient about 1mm(1×10^6nm). It shows that the luminescence intensity away from the Rb-L edge increases as a linear function for thickness for the most part. But it near edge is nearly saturated beyond the certain thickness, as the difference value between the edge intensity and off-edge on the sample A is nearly same as that on the sample B. In other words, the excitation spectrum of RbBr changes the feature depending on the thickness. On the other hand, the excitation spectrum of the other alkali bromides increases as a linear function for thickness even in the absorption edge region. This is a strange behavior and becomes a new question for us. Some further studies are needed for this luminescence problem.

Fig.2

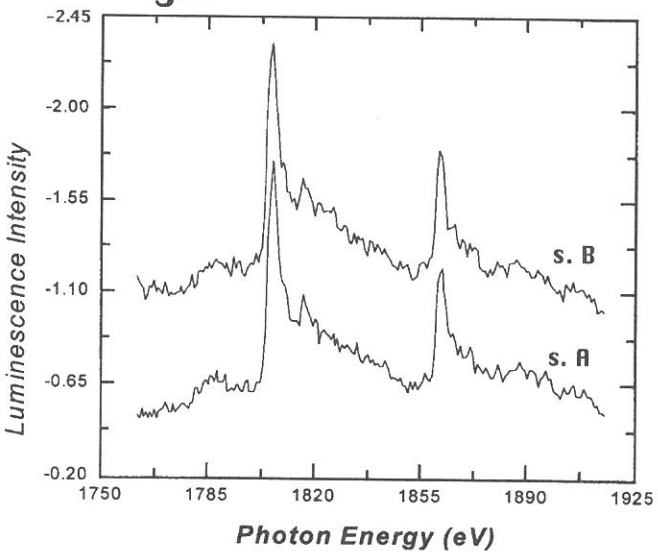

Fig.3

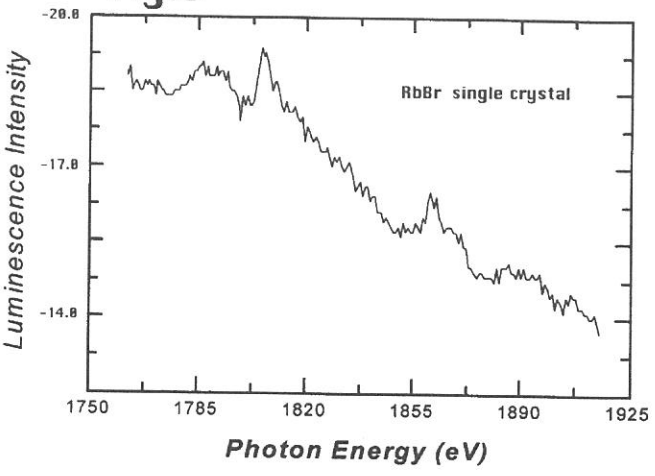

(BL7A)

Thickness Effects of Photoluminescence from Sodium Bromide Film Excited with Soft X-Rays in Na-K Edge Energy

Masahiro MORI, Takashi IKEDA, Takaaki AWATA[‡] and Tokuo MATSUKAWA[‡]

School of Informatics and Sciences, Nagoya University, Nagoya 464-8601
[‡] *Naruto University of Education, Naruto, Tokushima 772-8502*

(5: Solid- & liquid-phase spectroscopy 2; soft x-ray, absorption, photo-luminescence)

We have measured sample thickness dependence of photoluminescence excitation spectra from vacuum evaporated NaBr film excited near the photon energy region of Na-K absorption edge. Na-K spectra have become possible to measure by the use of a beryl crystal as a practical monochromator crystal at BL7A beam line, UVSOR. We have obtained Na-K absorption spectra of sodium halides by the transmission methods and photoluminescence yield spectra from thin samples excited in the energy region. In the case of fine powder samples, the excitation spectra show inverted profiles of absorption spectra in the case of NaBr fine powder sample, whereas other alkali bromides show same profile as the absorption spectra. It has been considered that it might depend on the absorption intensity, that is, the effective sample thickness. The purpose is to observe the relation between sample thickness and excitation spectrum. The excitation spectra were measured on NaBr thin films prepared by vacuum evaporation with different thickness. Although their results do not always show an existence of inverted feature, the intensity of excitation spectra are found to show characteristic variation with sample thickness.

Experiments were performed at the BL7A with a beryl monochromator crystal near the photon energy region of Na-K absorption edge. Several modifications were applied for the beam line. A sample preparation chamber was attached to the sample chamber to evaporate samples in a separated place. Samples were prepared with vacuum evaporation on to a polyester 2μm thin film and transferred to the experimental chamber for each measurements on every sample with different thickness. All measurements were carried out at room temperature. Evaporations were repeated over the one same sample film after a measurement. The thickness of the evaporated sample film was monitored by a quartz thickness monitor and was given by the frequency shift.

A photo-multiplier tube was installed at 45 degrees to incident light direction through a quartz focusing lens of 20mm diameter at 200mm from the sample position. The absorption spectra were obtained by the total photoelectron yield. An electron-multiplier with a Be-Cu anode was set behind the sample film, and absorption spectra were simultaneously obtained by a transmission method getting along with the excitation spectra.

Figure 1 shows the excitation spectrum on sodium bromide excited with a soft x-ray near Na-K edge energy. Spectral features are all common among the samples with the different thickness and with the absorption spectrum except the intensity distribution. As the thickness are small, it is apparent that the photoluminescence intensity increases rapidly.

Figure 2 shows a change of luminescence intensity measured at the energy below the absorption edge, the first, second, third absorption peak and forth peak, which are shown by arrow A, B, C, D and E in Fig. 1, respectively.

Fig.1

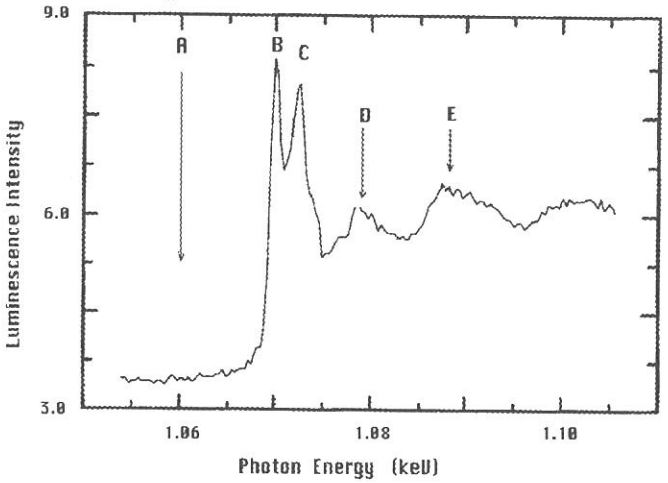

Intensity of the photoluminescence from the thin film, excited with a soft x-ray, is nearly zero independent from sample thickness for very thin thickness, and increases as a linear function for thick. It seems that quantum efficiency curves of A, B, C, D and E are same with each other except their intensity nomalization. It is strange. Because the luminescence intensity depends on the whole amount of creation of inner core holes, and the amount may depends on dose of absorbed x-ray, thus it should be considered to be proportional to the thickness of the sample. The intensity of the light may be unchanged since alkali halides are transparent in visible and UV region, thus no self absorption effects are considered. We have obtained quantum efficiency spectra, ratio spectra of the luminescence and the dose spectra. The dose spectra are given by $(I_0 - I)$ spectra, where I_0 is incident x-ray spectra and I is transmitted x-ray spectra. It shows that all quantum efficiency of A, B, C, D and E are not only linearly changes against the sample thickness as the samples are thin, but also they appear to converge to zero at thickness of about 25nm commonly among A, B, C, D and E. If it is true, it suggests that there is a threshold in the sample thickness to excite the photoluminescence by x-ray.

Fig.2

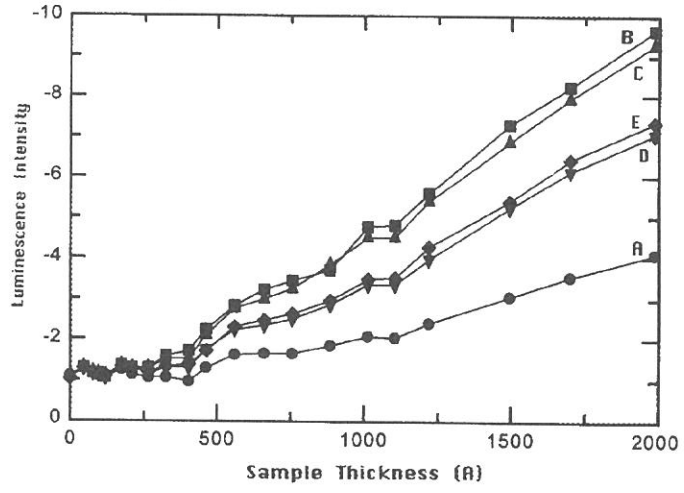

(BL7A)

An electronic static study on the analysis of Al *K* X-ray Absorption Near Edge Structure for Aluminum complexes

K. Shirozu, S. Matsuo, T. Kurisaki, T. Yokoyama, H. Wakita

Department of Chemistry, Faculty of Science, Fukuoka University, Nanakuma, Jonan-ku, Fukuoka 814-0180, Japan

Department of Chemistry, Faculty of Science, Kyushu University, Hakozaki, Higashi-ku, fukuoka 812-8581, Japan

【Introduction】

The characterization of aluminum is one of the most important study in the field of ceramics and glasses. The NMR spectroscopy is a powerful method for studying Al^{3+} complexes in the solution and solid states. In addition to ^{1}H- and ^{13}C- NMR spectra, ^{27}Al- NMR spectra can be obtained in relatively straightforward manner. The chemical shift of NMR spectra is caused by shielding of the magnetic field by electron around nuclear; i.e. the chemical shift depends on the electron density around nuclear.

In this study, the Al *K* XANES spectra of several aluminum complexes, which have different coordinated atoms each other, were measured and discussed the electronic structures. Moreover, electron density of aluminum compounds is analyzed by using a DV-Xα MO calculation, and discussed the correlation between chemical shift of NMR and the result of XANES spectra.

【Experiment and calculation】

The samples of this study are Al(EDTA), Al(lactate) and Al(pentanedionate). Al(EDTA) contains six coordinate Al3+ ions, each of which is bonded to two N atoms and four O atoms. Al(lactate) and Al(pentanedionate) have sixfold coordination, by six O atoms. The Al *K* XANES spectra were collected on the BL7A at the UVSOR of the Institute for Molecular Science in Japan using two KTP(001) monochromator crystals. The storage ring was operating at the electron energy of 750 MeV. All of XANES spectra were detected by a total electron yield method. Based on crystal structures of Na[Ga(EDTA)], [Al(Lactate)] and [Al(Pentanedionate)], the model structures of Na[Al(EDTA)] [Al(Lactate)] and [Al(Pentanedionate)] were constructed for the DV-Xα MO calculation, respectively.

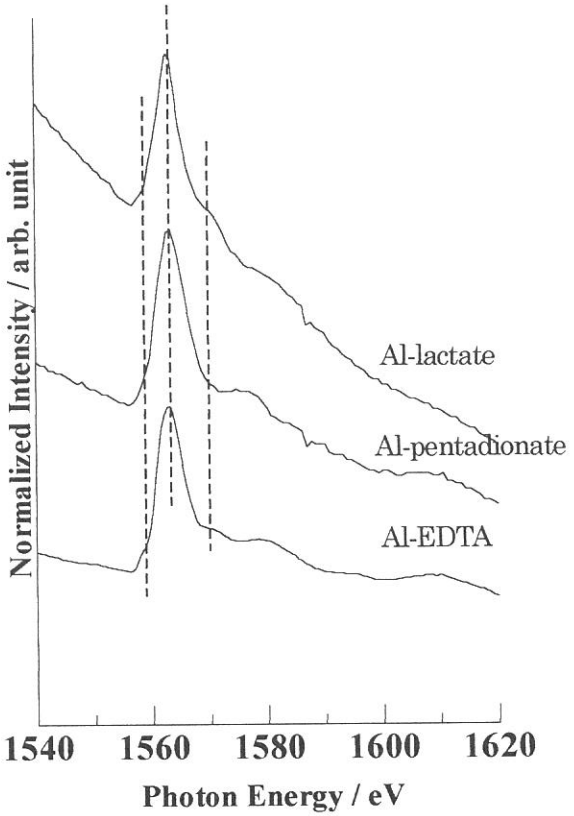

Fig.1 The Al K XANES spectra of aluminum complexes

【Results and discussion】

The Al *K* XANES spectra of these compounds are shown in Fig. 1. For Al *K* XANES spectra, the first peak of *K*-edge shifts higher energy with increasing the coordination numbers of aluminum ions. The absorption edges of three compounds are located on the same energy level. Thus their compounds have the same coordination number. Furthermore, the shapes of XANES spectra are similar to each other, so it can be presumed that there compounds have similar surroundings of aluminum ions. From the result of NMR spectra, the chemical shift of compounds is increasing as follows; Al(lactate) < Al(pentanedionate) < Al(EDTA). Therefore, Al(EDTA) has the poorest electron density of aluminum. We have analyzed the Al *K* XANES spectra of these compounds by a DV-Xα MO calculation. The electron density which was obtained by the DV-Xα MO calculation is increasing in order; Al(lactate) > Al(pentanedionate) > Al(EDTA). So the correlation between the chemical shift and electron density which obtained from XANES spectra analysis is observed in only these three compounds. Further measurement and theoretical study are required.

(BL7A)

A structural study on analysis of Al *K* X-ray Absorption Near Edge Structure for Aluminum complexes with carboxylamine

K. Shirozu, S. Matsuo, T. Kurisaki, T. Yokoyama, H. Wakita

Department of Chemistry, Faculty of Science, Fukuoka University, Nanakuma, Jonan-ku, Fukuoka 814-0180, Japan
Department of Chemistry, Faculty of Science, Kyushu University, Hakozaki, Higashi-ku, fukuoka 812-8581, Japan

【Introduction】

Fulvic acid is a major organic compound in soil solution, and the interaction between this acid and aluminumgives some influence to the behavior of aluminum. Therefore, it is important to understand the behavior of aluminum with this acid on the environmental sciences. Thus for understanding the binding properties of aluminum ion to fulvic acid, it is also important to investigate the interaction between aluminum ion and some model compounds of fulvic acid including carboxyl and amino groups in aqueous solution. We choose EDTA and CyDTA as the model compounds. But the structure of aluminum complexes with these model compounds was not clear yet. As the first step to understand the interaction between aluminum ion and model compounds in aqueous solution, we analyzed the Al *K* XANES spectra of two aluminum complexes using DV-Xα MO calculation, and discussed electronic and steric structure of those complexes in solid state.

【Experiment and calculation】

The Al *K* XANES spectra were collected on the BL7A at the UVSOR of the Institute for Molecular Science in Japan using two KTP(001) monochromator crystals. The storage ring was operating at the electron energy of 750 MeV. All of XANES spectra were detected by a total electron yield method. Based on crystal structures of Na[Ga(EDTA)] and K[Al(CyDTA)], the model structures of Na[Al(EDTA)] and K[Al(CyDTA)] for the DV-Xα MO calculation were constructed, respectively (Fig.1 and 2).

【Result and discussion】

The Al *K* XANES spectra of these compounds are shown in Fig. 3 and 4, and are represented by solid line. The absorption edges of two compounds are located on the same energy level. Furthermore, the shapes of XANES spectra are similar to each other, so it can be presumed that two compounds have the same surroundings of aluminum ions. The DV-Xα calculation was performed for two compounds. The obtained results were shown in Fig. 1 and 2, where straight lines are the probability of electron transition, broken lines are the calculated XANES spectra which were obtained by the probability of electron transition. For the two compounds, calculated XANES spectra reproduce experimental XANES spectra well. From this result, model structures for DV-Xα calculation were thought to be valid. Furthermore from the result of DV-Xα calculation, it is clear that

electron density of aluminum of Al(CyDTA) is more dense than that of Al(EDTA). Bond length of Al-O in Al(CyDTA) is shorter than that in Al(EDTA). This difference of bond length occurs by the difference of flexibility, which is caused by the difference between cyclohexane and ethylene in CyDTA and EDTA, respectively. Shorter the bond length, larger the relative electron density. Thus by not only the coordinated atom but also the degree of flexibility of the ligand, the electronic state of aluminum is influenced

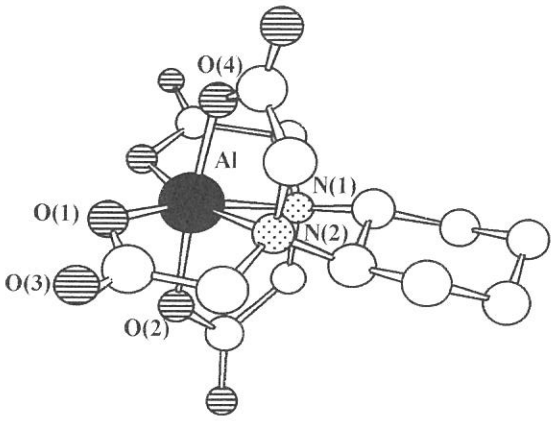

Fig. 1 The model structure of [Al(CyDTA)] for DV-Xα calculation.

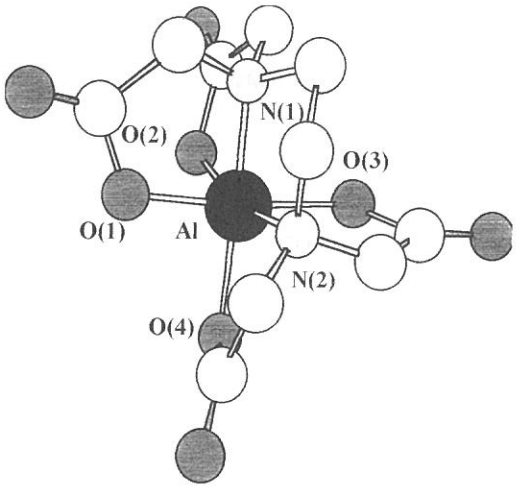

Fig. 2 The model structure of [Al(EDTA)] for DV-Xα calculation.

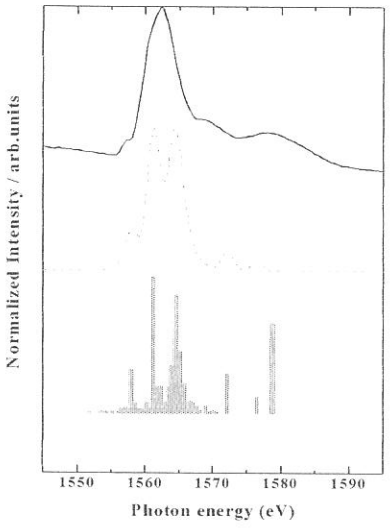

Fig. 3 Experimental and calculated Al *K* XANES spectra of [Al(CyDTA)]

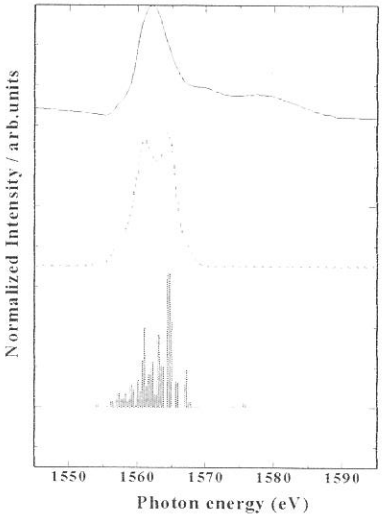

Fig. 4 Experimental and calculated Al *K* XANES spectra of [Al(EDTA)]

(BL8B1)

Changes in Electronic Structure by Li Ion Deintercalation in $LiCoO_2$ From Cobalt *L*-edge and Oxygen *K*-edge XANES

Yoshiharu Uchimoto
Department of Applied Chemistry, Graduate School of Science and Engineering, Tokyo Institute of Technology
Ookayama, Meguro, Tokyo 152-8552, Japan.

Lithium cobalt oxide, $LiCoO_2$, is used as the cathode active material in commercially available 4V-type lithium secondary because of its high theoretical energy density and good cycle performance. In the lithium secondary batteries, which are called 'rocking-chair' batteries, graphite is used as the negative electrode. During the charge and discharge process, lithium ions are transferred from one electrode to the other electrode through an intercalation and/or de-intercalation process. It is important to clarify the change of electronic structure during the charge and discharge process in order to understand the electrochemical properties. Recently first principle molecular orbital calculation studies of the electronic structure of the $Li_{1-x}CoO_2$ have been reported (1, 2). These calculation results indicate that the lithium ion deintercalation increases the covalent interaction between cobalt and oxygen and that the oxidation associated with the deintercalation mainly takes place on oxygen. However experimental information about the electronic structure change during the lithium ion deintercalation is insufficient. To our knowledge, the detailed electronic structure change during electrochemically intercalation and/or de-intercalation process has not yet been reported.

In this study, a measurement of cobalt L_{23}-edge and oxygen K-edge XANES was used to determine the electronic structure changes of $LiCoO_2$ during the electrochemical lithium ion deintercalation.

$LiCoO_2$ powder was prepared by conventional solid state reaction starting with lithium hydroxide (Wako Chemical Co. Inc., 99.9%) and cobalt hydroxide (Wako Chemical Co. Inc., 99.9%). A mixture of Li(OH) and $Co(OH)_2$ in a mole ratio of 1:1 was heated at 700℃ for 13 h in air atmosphere. The crystal structure of the product was determined by XRD using Mo-Ka radiation. $Li_{1-x}CoO_2$ oxides were prepared by electrochemical lithium de-intercalation. A mixture of 82.5 wt% $LiCoO_2$, 15 wt% acetylene black, and 2.5 wt% polytetrafluoropropylene binder was used as working electrode. Lithium metal was used as counter and reference electrode. The electrolyte was 1*M* lithium perchlorate in propylene carbonate solution.

Co L_{23}-edge XANES and oxygen *K*-edge XANES were measured on BL-8B1 beam line at UVSOR (Okazaki, Japan) with ring energy of 750 MeV in a mode of total electron yield at room temperature, respectively.

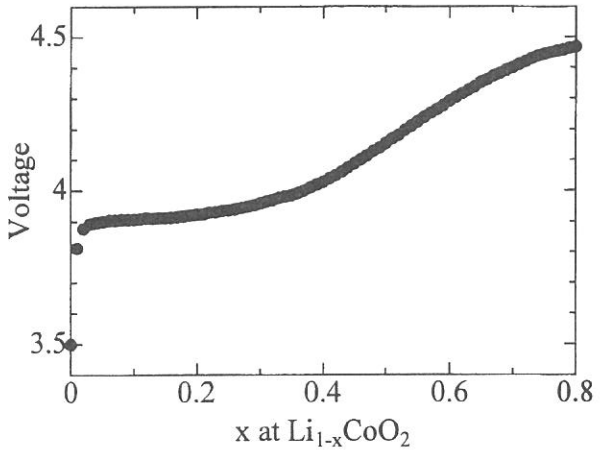

Figure 1
Electrode potential change of the $Li_{1-x}CoO_2$ electrode during the charge process.

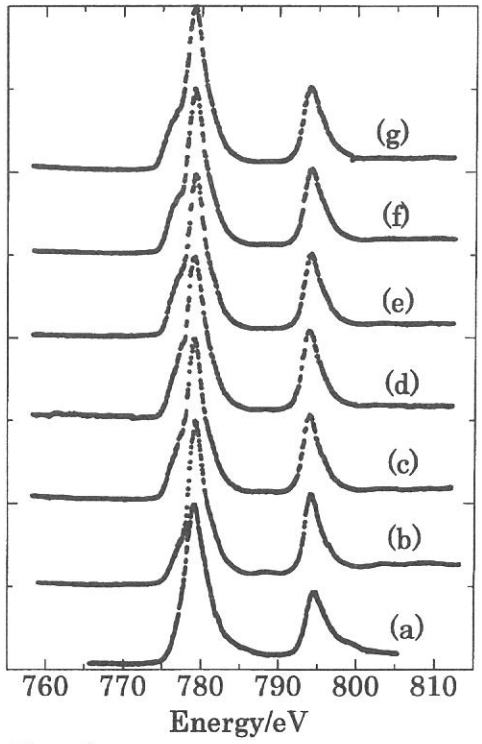

Figure 2
Co 2p absorption spectra of $LaCoO_3$ (a) and $Li_{1-x}CoO_2$ (b-g).
(b) 1.0, (c) 0.8, (d) 0.6, (e) 05, (f) 0.4, (g) 0.2

The XRD pattern of $LiCoO_2$ was indexed to a rhombohedral lattice and is in good agreement of that of $LiCoO_2$ (*R3m*). Figure 1 shows the electrode potential change during the electrochemical extraction of lithium from $LiCoO_2$ in the region from x = 0 to x = 0.8 of $Li_{1-x}CoO_2$. The electrode potential change is in good agreement with the open circuit voltage curve of $Li_{1-x}CoO_2$ reported by Mizushima et.al. (3).

Figure 2 shows the Co *L*-edge XANES of $Li_{1-x}CoO_2$ at various x values together with that of $LaCoO_3$ as model compounds of Co^{3+} oxidation state. The Co *L*-edge XANES shows two strong absorption features due to the spin-orbit splitting of the Co 2p core hole (Abbate *et al.*, 1993). The absorption about 779 eV is $2p_{3/2}$ (L_3) edge and that about 794 eV is $2p_{1/2}$ (L_2) edge. The Co *L*-edge XANES of $LiCoO_2$ is in good agreement that reported by Montoro et.al (4). The shape of the Co *L*-edge XANES of $LiCoO_2$ and $LaCoO_3$ close similarity of low-spin Co^{3+} (4). The Co *L*-edge spectra of $Li_{1-x}CoO_2$ (x=0.2, 0.4, 0.5, 0.6, 0.8, 1.0) do not exhibit chemical shift and the changes of the shape are small. The result that the XANES did not show any chemical shift indicates the Co ion in the $Li_{1-x}CoO_2$ is still trivalent Co^{3+} cations even at low x value of 0.2.

Figure 3 shows the oxygen K-edge XANES of $Li_{1-x}CoO_2$ at various x values. A peak at about 528-530 eV is attributed to transration to the unoccupied band derived from the mixing of the Co 3d states with oxygen 2p states. The broad structure about 535-550 eV is attributed to band of Co 4s and/or 4p character. The peak is broad, so that the peak is difficult to divide two characters. Figure 4 shows a magnified part of Figure 3 between 525 and 535 eV. The peak at about 527 eV increases with decreasing lithium content. This result shows that oxidation also takes place on oxygen 2p orbital and the ground state of $Li_{1-x}CoO_2$ is $Co^{3+}\underline{L}$, where $\underline{L}$ represents a ligand hole state. This phenomenon indicates that the oxidation by anode reaction of lithium deintercalation mainly takes place by using oxygen 2p orbital but Co 3d orbital. This is in good agreement with the result of First-Principles calculation for $Li_{1-x}CoO_2$ oxides (2).

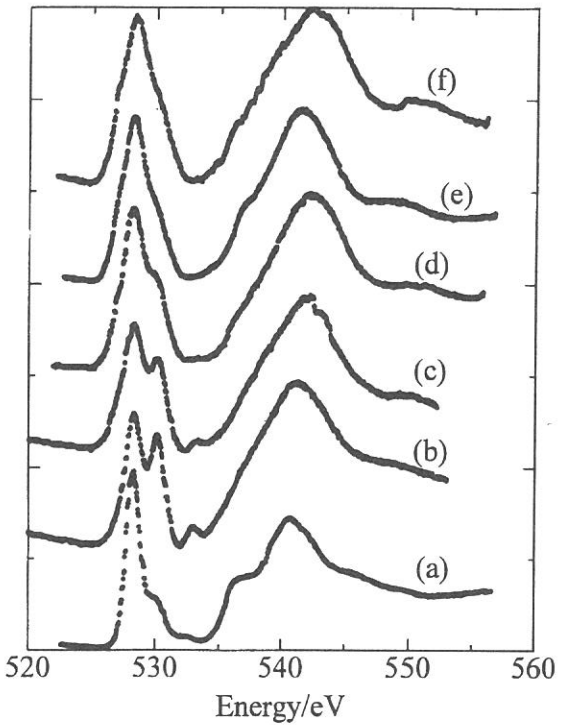

Figure 3
O 1s absorption spectra of $Li_{1-x}CoO_2$.
(a)1.0, (b) 0.8, (c) 0.6, (d) 05, (e) 0.4, (f) 0.2

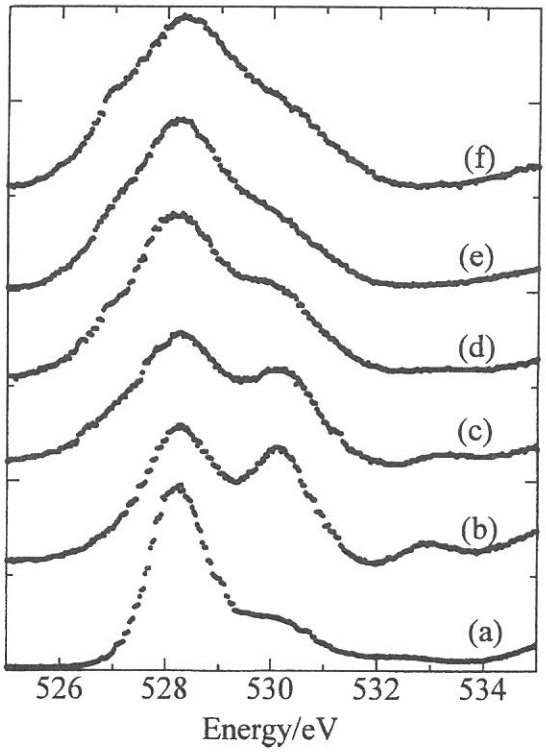

Figure 4
O 1s absorption spectra of $Li_{1-x}CoO_2$ between 525 and 535eV.
(a)1.0, (b) 0.8, (c) 0.6, (d) 05, (e) 0.4, (f) 0.2

References

1) Aydiol, M.K., Kohan, A.F., Cedar, G., Cho, K., & Joannopoulos, J., (1997). *Phys. Review B,* **56**, 1354-1365.

2) Koyama, Y., Tanaka, I., Kim, Y.S., Nishitani, S.R., & Adachi, H., (1999). *Jpn. J. Appl. Pys.*, **38**, 4804-4808.

3) Mizushima,K., Jones, P.C., Wiseman, P.J., & Goodenough, J.B., (1980). *Mater. Res. Bull.*, **15**, 783-789.

4) Montoro, L.A., Abbate, M., Almeida, E.C., & Rosolen, J.M., (1999) *Chem. Phys. Lett.*, **309**, 14-17.

(BL8B2)

Electronic structure and molecular orientation at the surface of poly(9-vinylcarbazole) thin film studied by angle-resolved ultraviolet photoelectron spectroscopy

K.K.Okudaira, Y.Azuma, S.Hasegawa[A], K.Seki[B], and N.Ueno[C]

Graduate School of Science and Technology, Chiba University, Chiba 263-8522
[A]Institute for Molecular Science. Okazaki, 444-8585
[B]Faculty of Science, Nagoya University, Nagoya 464-8602
[C]Department of Materials technology, Faculty of Engineering, Chiba University, Chiba 263-8522

Thin films of pendant group polymers are widely used in practical applications due to molecular stability and facility of preparation. Since the properties of organic devices consisting of the films depend strongly on the molecular orientation at the film surfaces, determination of the surface molecular orientation such as tilt angle distribution of pendant group is very important for understanding the device properties.

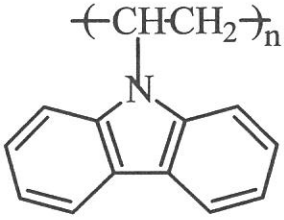

Figure 1 Molecular structure of poly(9-vinylcarbazole)

Angle-resolved ultraviolet photoelectron spectroscopy (ARUPS) using synchrotron radiation offers information on the geometrical structure of thin films as well as on their electronic structures. From the comparison between ARUPS and near-edge X-ray absorption fine structure (NEXAFS) of poly(2-vinylnaphthalene) (PvNp) thin film, we showed that the tilt angle distribution of the pendant groups of PvNp is well described by the three-dimensional isotropic random orientation. [1]

In the report, we investigated the orientation of pendant groups at the surface of poly(9-vinylcarbazole) (PvCz) [see Fig. 1] thin film using ARUPS and NEXAFS spectroscopy. The pendant carbazole group of PvCz has a large π electron system as PvNp. However, it has a larger heterocyclic ring in comparison with the pendant naphthalene group of PvNp. The surface pendant-group orientation of PvCz film is thus expected to be different from that of PvNp.

ARUPS measurements were carried out at the beamline BL8B2 of the UVSOR at the Institute for Molecular Science. ARUPS spectra were measured at hν=40eV and at normal incidence (incidence angle of photon α=0°). Thin films of PvCz were prepared by spincasting on Au-evaporated Si(100) wafers from toluene solutions of 0.3wt/vol%. The film thickness prepared in this way is about 100Å.

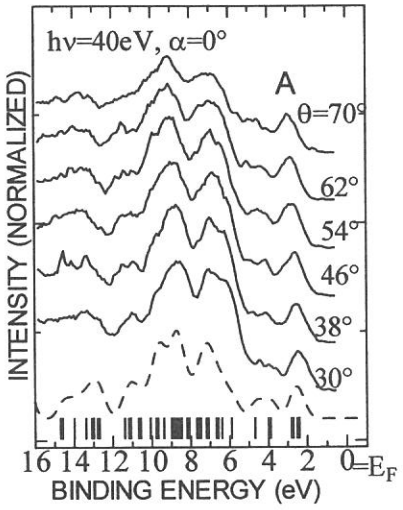

Figure 2 ARUPS of PvCz thin films spincasted from 0.3 wt/vol% toluene solution at hν=40eV and α=0° as a function of take-off angle (θ). The vertical bars show the molecular orbital energies calculated by *ab initio* MO calculation (STO-6G). The density of states (DOS) is represented by (– – – – –) (see text). The calculated binding energy scale was contracted by 1.35 and shifted to fit with the experimental results.

Figure 2 shows the ARUPS spectra of the PvCz thin film as a function of the take-off angle (θ). The intensity of top band A shows slight θ dependence. The calculated density-of-states (DOS) using molecular orbital (MO) calculation (STO-6G) is also shown in Fig.2. The MO calculation was performed for a model compound [CH_3-CH($NC_{12}H_8$)-CH_3] of the polymer unit, and the DOS was obtained by a Gaussian broadening (FWHM = 0.8 eV) of the MO levels. The agreement between the observed spectra and the DOS indicates that the electronic structure of PvCz is well simulated by that of

the model compound. The band A in the spectra originates from two top π states at the pendant carbazole and hereafter we focus on the θ dependence of the intensity of the band A to determine the orientation of the pendant carbazole groups at the surface.

In order to obtain the molecular orientation of the pendant carbazole, we made the analyses of the θ dependence in the single-scattering approximation combined with molecular orbital (SS/MO) approximation.[2] The calculations were performed for the model compound. The phase shift and radial matrix element were calculated for all subshells of the atoms constituting the molecules using the Muffin-tin potential,[3] and the potential between the Muffin-tin spheres was assumed to be zero. In the present calculation we used the phenomenological electron mean-free path of 8 Å to calculate the damping factor.[4] We further assumed an azimuthal disorder for the rotational orientation of the pendant carbazole groups with respect to the surface normal. For the calculation of photoelectron intensity, we introduced an inclination angle (β) of the molecular plane of pendant carbazole groups with respect to the film surface.

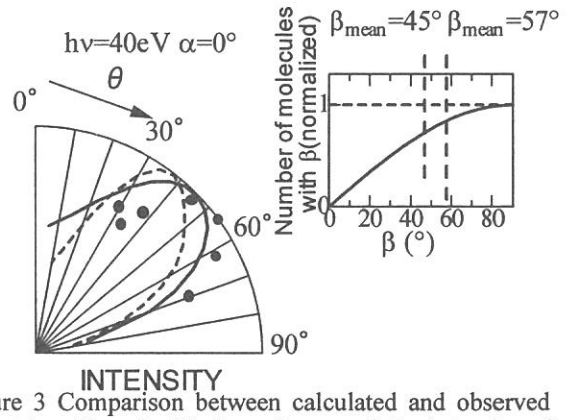

Figure 3 Comparison between calculated and observed (●) take-off angle (θ) dependences of the intensity of the band A. All calculations were carried out by the SS/MO approximation. The calculated result for 3-dimensional isotropic orientation (model 1) shown in the inset is represented by (———). The calculated result for an orientation where an orientation where the tilt angel β varies between 0° and 90° with the uniform distribution (model 2) is represented by (– – – – –). For each model, the β dependence of the number of molecules is shown in the inset.

In Fig. 3, the observed θ dependence of the intensity of the band A is compared with calculated results for two orientation models, namely (1); three-dimensional isotropic random orientation model which has a mean β value (β_{mean}) of 57°, and (2) an orientation model where the tilt angel β varies between 0° and 90° with the uniform distribution; thus β_{mean} = 45°. The calculated θ pattern for the model 1 is in better agreement with observed one than that for the model 2. It should be noted, however, that the observed θ dependence peaks clearly at larger θ than the calculated one for the model 1. It indicates that at the surface of PvCz film there are more pendant groups with large tilt angles than the orientation model 1. This different pendant-group orientation between PvCz and PvNp film can be ascribed to the difference in the size and chemical structure of pendant groups.

The β value of 60° determined by the NEAXFS study (not shown) is slightly larger than β_{mean} of 57° for the model 1. This result is consistent with that obtained from the ARUPS analyses. The present results indicate that the surface electronic states of PvCz may be rather dominated by σ(C-H) states at the pendant carbazole group than π states.

REFERENCES

[1]E.Morikawa, V.Saile, K. K. Okudaira, Y.Azuma, K.Meguro, Y.Harada, K.Seki, S.Hasegawa, and N.Ueno, J. Chem. Phys. **112** 10476(2000)

[2]N.Ueno, A.Kitamura, K.K.Okudaira, T.Miyamae, S.Hasegawa, H.Ishii, H.Inokuchi, T.Fujikawa, T.Miyazaki, and K.Seki, J.Chem.Phys., **107** 2079(1997).

[3]D.Dill and J.L.Dehmer, J.Chem.Phys., **61** 692 (1974).

[4]K. K. Okudaira, E. Morikawa, D.A.Hite, S. Hasegawa, H. Ishii, M. Imamura, H. Shimada, Y. Azuma, K. Meguro, Y. Harada, V. Saile, K. Seki, and N. Ueno, J.Electron Spectrosc.Relat.Phenom. 101-103, **389**(1999).

(BL8B1)

Changes in Electronic Structure by Li Ion Deintercalation in $LiNiO_2$ from Nickel *L*-edge and O *K*-edge XANES

Yoshiharu Uchimoto
Department of Applied Chemistry, Graduate School of Science and Engineering, Tokyo Institute of Technology
Ookayama, Meguro, Tokyo 152-8552, Japan.

$LiNiO_2$ oxide with a layered α-$NaFeO_2$ structure is one of the most promising cathode materials used in 4V-type lithium ion batteries because its low cost and high theoretical energy density. It is important to clarify the change of electronic structure during charge and discharge process in order to understand the electrochemical properties. Recently, first-principle molecular orbital calculations of the electronic structure of the $Li_{1-x}NiO_2$ have indicated that lithium ion deintercalation increases the covalent interaction between Ni and oxygen, and that the oxidation associated with the deintercalation mainly takes place on oxygen. [1-2] However, experimental studies of the electronic structure change during the lithium ion deintercalation are insufficient.In this study, Ni $L_{2,3}$-edge and O *K*-edge X-ray Absorption Near Edge Structure (XANES) was determined the electronic structure of $LiNiO_2$ during lithium ion deintercalation.

$LiNiO_2$ powder was prepared by conventional solid state reaction starting with lithium hydroxide (Wako Chemical Co. Inc., 99.9%) and nickel hydroxide (Wako Chemical Co. Inc., 99.9%). A mixture of Li(OH) and $Ni(OH)_2$ in a mole ratio of 1:1 was heated at 770°C for 30 h in an oxygen atmosphere. The crystal structure of the product was determined by XRD using Mo-K radiation. Li_xNiO_2 was prepared by electrochemical lithium deintercalation. A mixture of 82.5 wt% $LiNiO_2$, 15 wt% acetylene black, and 2.5 wt% polytetrafluoropropylene binder was used as working electrode. The electrolyte was a 1*M* $LiClO_4$ in PC solution. Ni $L_{2,3}$-edge XANES spectra were measured on the BL-7A beam line and O *K*-edge XANES were measured on the BL-8B1 beam line at UVSOR (Okazaki, Japan) with a ring energy of 750 MeV in a mode of total electron yield at room temperature.

The XRD pattern for $LiNiO_2$ was indexed in a rhombohedral *R3m* space group. The first-cycle discharge capacity is 140 mAh g^{-1}. Fig. 1 shows the Ni *L*-edge XANES of Li_xNiO_2 for various x values. The Ni *L*-edge XANES shows two strong absorption features of the spin-orbit splitting of the Ni 2p core hole. [3] The absorption near 852-856 eV is the $2p_{3/2}$ (*L3*) edge and that near 868-872 eV is the $2p_{1/2}$ (*L2*) edge. The XANES for $LiNiO_2$ is similar to that for NiO, which shows the Ni ions in $LiNiO_2$ to be Ni^{2+} ions in a high-spin state. [4] The spectra for Li_xNiO_2 (x=0.2, 0.4, 0.5, 0.6, 0.7, 0.8, 0.9, 1.0) do not exhibit chemical shift and the change in shape are small, indicating the Ni ion in the Li_xNiO_2 is still Ni^{2+} even at as low an x value as 0.2.

Fig. 2 shows the O *K*-edge XANES for Li_xNiO_2 for various x values. The peak at about 532 eV (●) is attributed to oxygen in the substrate. A peak at about 533 eV is attributed to the band derived from the mixing of the Ni 3d states with O 2p states. The broad structure near 535-550 eV is attributed to a Ni band with 4sp character. The peak at near 528 eV increased with decreasing lithium content. This result shows that oxidation influences the oxygen 2p orbital and the ground state of Li_xNiO_2 ($x<1.0$) is $Ni^{2+}\underline{L}$, where $\underline{L}$ represents a ligand hole state. [4] This indicates that the lithium deintercalation reaction does not involve Ni but oxygen.

REFERENCES

1) M.K. Aydinol, A.F. Kohan and G. Cedar, *J. Power Sources*, **68**, 664(1997).
2) Y. Koyama, Y.S. Kim, I. Tanaka and H. Adachi, *Jpn. J. Appl. Pys.*, **38**, 2024 (1999).
3) J. van Elp, B.G. Searle, G.A. Sawatzky and M. Sacchi, *Solid State Communication*, **80**, 67 (1991).
4) P. Kuiper, G. Kruizinga, J. Ghijsen, G.A. Sawatzky and H. Verweij, *Phys. Rev. Lett.*, **62**, 221 (1989).

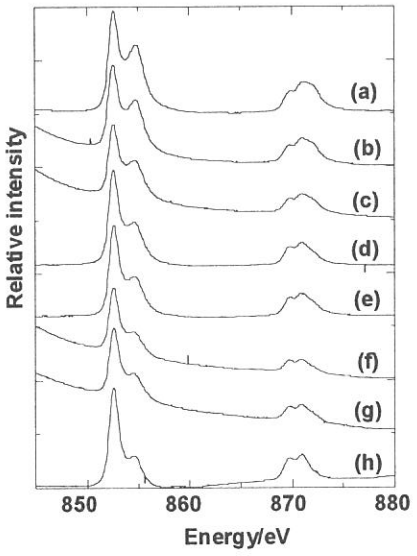

Fig. 1 Ni 2p absorption spectra for Li_xNiO_2:
(a) 0.2, (b) 0.4, (c) 0.5, (d) 0.6, (e) 0.7, (f) 0.8, (g) 0.9, (h) 1.0

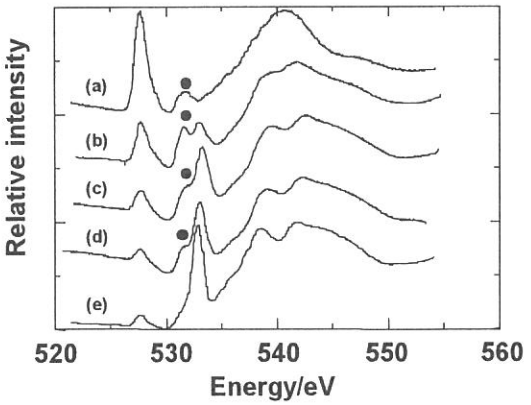

Fig. 2 O 1s absorption spectra for Li_xNiO_2:
(a) 0.2, (b) 0.5, (c) 0.6, (d) 0.8, (e) 1.0